Drug Design, Development and Therapy

Dovepress
open access to scientific and medical research

Open Access Full Text Article

ORIGINAL RESEARCH

Network and Experimental Pharmacology on Mechanism of Yixintai Regulates the TMAO/PKC/NF-κB Signaling Pathway in Treating Heart Failure

Ziyan Wang[1,2,*], Chengxin Liu[1,2,*], Jiaming Wei[2,3], Hui Yuan[1,2], Min Shi[2,3], Fei Zhang[2,3], Qinghua Zeng[2,3], Aisi Huang[2,3], Lixin Du[4], Ya Li[4], Zhihua Guo[2,3]

[1]First Clinical College of Chinese Medicine, Hunan University of Chinese Medicine, Changsha, 410208, People's Republic of China; [2]Hunan Key Laboratory of Colleges and Universities of Intelligent Traditional Chinese Medicine Diagnosis and Preventive Treatment of Chronic Diseases of Hunan Universities of Chinese Medicine, Hunan University of Chinese Medicine, Changsha, 410208, People's Republic of China; [3]School of Traditional Chinese Medicine, Hunan University of Chinese Medicine, Changsha, 410208, People's Republic of China; [4]School of Pharmacy, Hunan University of Chinese Medicine, Changsha, 410208, People's Republic of China

*These authors contributed equally to this work

Correspondence: Ya Li; Zhihua Guo, Email 003872@hnucm.edu.cn; 004294@hnucm.edu.cn

Objective: This study aims to explore the mechanism of action of Yixintai in treating chronic ischemic heart failure by combining bioinformatics and experimental validation.

Materials and Methods: Five potential drugs for treating heart failure were obtained from Yixintai (YXT) through early mass spectrometry detection. The targets of YXT for treating heart failure were obtained by a search of online databases. Gene ontology (GO) functional enrichment analysis and Kyoto encyclopedia of genes and genomes (KEGG) pathway enrichment analyses were conducted on the common targets using the DAVID database. A rat heart failure model was established by ligating the anterior descending branch of the left coronary artery. A small animal color Doppler ultrasound imaging system detected cardiac function indicators. Hematoxylin-eosin (HE), Masson's, and electron microscopy were used to observe the pathological morphology of the myocardium in rats with heart failure. The network pharmacology analysis results were validated by ELISA, qPCR, and Western blotting.

Results: A total of 107 effective targets were obtained by combining compound targets and eliminating duplicate values. PPI analysis showed that inflammation-related proteins (TNF and IL1B) were key targets for treating heart failure, and KEGG enrichment suggested that NF-κB signaling pathway was a key pathway for YXT treatment of heart failure. Animal model validation results indicated the following: YXT can significantly reduce the content of intestinal microbiota metabolites such as trimethylamine oxide (TMAO) and improve heart failure by improving the EF and FS values of heart ultrasound in rats and reducing the levels of serum NT-proBNP, ANP, and BNP to improve heart failure. Together, YXT can inhibit cardiac muscle hypertrophy and fibrosis in rats and improve myocardial ultrastructure and serum IL-1β, IL-6, and TNF-α levels. These effects are achieved by inhibiting the expressions of NF-κB and PKC.

Conclusion: YXT regulates the TMAO/PKC/NF-κB signaling pathway in heart failure.

Keywords: heart failure, yixintai, TMAO, PKC/NF-κB pathway, traditional Chinese medicine, network pharmacology

Introduction

Heart failure (HF) is the primary cause of death in patients with cardiovascular disease.[1] HF is characterized by heart structural or functional failure, leading to impaired ventricular filling and ejection function, inability of the heart to provide sufficient blood to tissues to meet metabolic needs, pulmonary and systemic circulation congestion, and organ and tissue perfusion. Clinical manifestations include dyspnea, physical activity limitation, and fluid retention. Approximately 2% of adults globally have HF, with poor prognosis and high hospitalization and mortality rates.[2] Despite significant progress in

Received: 29 December 2023
Accepted: 16 April 2024
Published: 30 April 2024

treating heart failure, patient readmission and cardiac events remain high. Therefore, it is crucial to research and develop drugs for HF.[3,4] Many studies have demonstrated the impact of the gut microbiota on HF pathogenesis, and the substances secreted by the gut microbiota are closely related to HF occurrence and progression. Multiple studies have shown a close relationship between intestinal microbiota secretion, trimethylamine oxide (TMAO), and HF occurrence and development.[5,6] Protein kinase C (PKC) is crucial in most G-protein-mediated receptors mediating biological effects and often acts upstream of nuclear factor kappa-B (NF-κB) by participating in IkB phosphorylation, which binds to NF-κB, dissociates, and causes NF-κB activation.[7] After activation, NF-κB is transferred into the nucleus to induce the expression of specific genes, activate the release of cytokines such as TNF-α, IL-1, and IL-6, and induce an inflammatory response, leading to cardiac hypertrophy, fibrosis, and HF.[8,9] Inhibiting the PKC/NF-κB pathway can improve angiotensin II–induced cardiomyocyte hypertrophy.[10] Moreover, TMAO activates protein kinase C (PKC)/NF-κB, which upregulates vascular cell adhesion molecule (VCAM-1) expression, directly leading to endothelial dysfunction.[11] Therefore, intervention in the TMAO/PKC/NF-κB pathway has potential value in treating HF.

Yixintai (YXT) is a commonly used traditional Chinese medicine (TCM) formula for treating HF in clinical practice. It has been used for nearly 20 years in the First and Second Affiliated Hospitals of the Hunan University of TCM. It comprises classic drug pairs, such as Astragalus membranaceus (Fisch.) Bunge, Salvia miltiorrhiza Bunge, Carthamus tinctorius L., Panax ginseng C. A. Mey, Alisma plantago-aquatica L., Polyporus umbellatus (Pers.) Fr., Draba nemorosa L., and Poria cocos(Schw) Wol. Its efficacy is to replenish qi, promote blood circulation, promote diuresis, and reduce swelling when combined with pharmacological and systemic biological methods. Network pharmacology predicts the possible mechanisms of TCM treatment effects. Network pharmacology has improved the ability to explore "multiple components and targets" of TCM, which is conducive to developing basic research on TCM and new drugs.[12]

Therefore, this study utilized network pharmacology to predict potential targets and signaling pathways related to HF. Furthermore, an HF model in SD rats was established by ligating the anterior descending branch of the left coronary artery (LAD) to verify the mechanism of action of YXT in treating HF.

Materials and Methods

YXT Preparation and High-Performance Liquid Chromatography (HPLC) Analysis

YXT is composed of eight herbal medicines, as shown in Table 1. Eight TCM extracts were extracted by EFONG Pharmaceutical Co., Ltd. (Guangdong, China) as formula granules; the batch numbers were Astragalus membranaceus (Fisch.) (batch number: 1051693) 30 g (1:5) = 6 g; Salvia miltiorrhiza Bunge (batch number: 1080473) 15 g (1:5.6) = 2.68, Carthamus tinctorius L. (batch number: 1081223) 5 g (1:6.3) = 0.79, Panax ginseng C. A. Mey (batch number: 1042233) 10 g (1:5) = 2 g, Alisma plantago-aquatica L. (batch number: 1081173) 10 g (1:6.7) = 1.49, Polyporus umbellatus (Pers.) Fr. (batch number: 1051953) 15 g (1:14.3) = 1.05, Draba nemorosa L. (batch number: 1042123) 15 g (1:20) = 0.75, Poria cocos(Schw) Wol (batch number: 1071523) 15 g (1:20) = 0.75, prepared according to the Chinese Pharmacopoeia (2015 edition) issued by the Chinese Pharmacopoeia Commission.

Based on the previous research foundation of our research group,[13] chromatography was performed using Agilent 1260 high-performance liquid chromatography (Agilent, USA). The separation was achieved on a Hypersil BDS C18

Table 1 Composition of YXT

Chinese Name	Botanical Name	Dosage(g)
Huangqi	*Astragalus membranaceus* (Fisch.) Bunge	6
Danshen	*Salvia miltiorrhiza* Bunge	2.68
Honghua	*Carthamus tinctorius* L.	0.79
Renshen	*Panax ginseng* C. A. Mey	2
Zexie	*Alisma plantago-aquatica* L.	1.49
Zhuling	*Polyporus umbellatus* (Pers.) Fr.	1.05
Tinglizi	*Draba nemorosa* L.	0.75
Fuling	*Poria cocos*(Schw) Wol	0.75

column (250 mm x 4.6 mm, 5 μm), employing a mobile phase consisting of 0.1% phosphoric acid in water (A) and methanol (B) in a gradient elution process: 0–25 min, 2% B to 22% B; 25–49 min, 22% B to 34% B; 49–57 min, 34% B to 42% B; 57–65 min, 42% B held constant; 65–73 min, 42% B to 50% B; 73–93 min, 50% B to 100% B; 93–103 min, 100% B to 5% B; 103–108 min, 5% B held constant. The flow rate was set at 1.0 mL/min, with a detection wavelength of 286 nm, column temperature maintained at 30 °C, and an injection volume of 10 μL.

A CP1.14 millionth electronic balance (Orhaus Instruments Co., Ltd., USA) was used to weigh 1.20 g of ten batches of YXT granules into a 10 mL volumetric flask, numbered S1–S10, and 50% ethanol aqueous solution was added to the mark. A KQ-400DE CNC ultrasonic cleaner (Kunshan Ultrasonic Instrument Co., Ltd., China) was utilized for 1 hour at 500 W and 40 kHz, followed by centrifugation at 12,000 rpm for 30 minutes using a TGL-16M high-speed freezing centrifuge (Nanping Technology Co., Ltd., China). The supernatant was then filtered through a 0.22μm filter and transferred into a sample bottle for usage. Subsequently, an appropriate amount of reference substances, including salvianolic acid B, hydroxysafflor A, calyx isoflavone, calyx isoflavone glucoside, and calyx anthocyanin, was added, and methanol was introduced to achieve mass concentrations of 63.6, 54.5, 81.8, 136.4, and 54.5 μg·mL–1, respectively, in the mixed reference solution.

Precision suction of the test sample supernatant exceeding 0.22 μm was required. The membrane was filtered into an injection bottle, and the sample was injected continuously six times, according to the chromatographic conditions. Using the peak of salvianolic acid B as a reference, we calculated the RSD of the relative peak area and relative retention time. The supernatant of the test sample was precisely suctioned through a 0.22 μm filter membrane into the injection bottle. The sample was then injected at 0, 6, 12, 24, 36, and 48 h in accordance with the specified chromatographic conditions, and the above experimental operation was repeated three times. Ten batches of YXT granules were used for testing, and a mixed reference solution was injected according to the chromatographic conditions. The chromatographic data of each batch of samples was imported into the "Similarity Evaluation System for Traditional Chinese Medicine Chromatographic Fingerprint (2012 Edition)" for analysis, confirmed the common characteristic peaks, and overlapped the mixed reference chromatogram with the sample fingerprint for identification. In the "Similarity Evaluation System for Traditional Chinese Medicine Chromatographic Fingerprint (2012 Edition)", S1 is used as the reference spectrum, with a time width of 0.15 set, and the median method is used to generate the fingerprint spectrum. Multiple point correction and mark matching were performed on the fingerprint spectrum, and ten batches of fingerprint patterns and similarity evaluation data for YXT granules were generated.

Analysis Based on Bioinformatics

In this study, early mass spectrometry detection identified five drugs with potential for heart failure intervention: Hydroxysafflor yellow A, calycosin-7-O-β-D-glucoside, salvianolic acid B, calycosin, and formononetin. These compounds were sourced from the PubChem database (https://pubchem.ncbi.nlm.nih.gov) to obtain either the primer or the SDF format of their 2D/3D structures. Subsequently, the SMILE or 2D/3D structures were imported into the Swiss Target Prediction database (http://www.swisstargetprediction.ch/predict.php) to identify the targets of the active ingredients in the drugs.

Using the Genecards database (https://www.genecards.org/), with a deep score > 1 for filters, the PKC-NFκB signaling pathway predominate targets were obtained. A total of 2052 PKC-NFκB signaling pathway targets were obtained from the Genecards database.Using the GEO database and the search term "Heart failure", the GSE591 chip expression matrix was obtained. GSM8979 and GSM8982-GSM8986 samples were divided into control (control) and GSM8987-GSM8998 samples into the HF group. We used the R language limma package to perform differential analysis of the expression matrix, removing probes corresponding to multiple molecules from one probe. Only the probe with the highest signal value was retained when probes corresponding to the same molecule were encountered. HF differentially expressed genes (DEGs) were screened using P.adj<0.05, logFC≥1, or logFC≤-1 as screening criteria. Using the R language ComplexHetmap package and Euclidean distance clustering method, the top 30 differential gene heatmaps were plotted based on the absolute value of logFC. The R language ggplot2 package was employed to draw volcano maps to observe differential gene expression effects. The R language ggplot2 package was used to draw box plots and PCA plots to observe the standardization and distribution of HF samples. The study involved human data from two public databases, Genecards and GEO. Due to the fact that GeneCards and GEO belong to public databases and users can download relevant data for free for research and publish relevant articles, the Medical Ethics Committee of The First Hospital of Hunan University of Chinese Medicine confirms that this study would have had the need for ethics approval waived.

To identify effective targets for drugs and HF DEGs, the PKC-NF-κB signaling pathway was the primary focus. Targets were imported into a bioinformatics database (http://bioinformatics.psb.ugent.be/cgi-bin/liste/Venn/calculate_venn.htpl) to ascertain differential genes, termed "potential DEGs", for drug intervention in heart failure. This process facilitated the creation of a Wayne diagram to visually map the intersection of these targets.

The species "Homo sapiens" was selected using multiple proteins in the STRING database (https://cn.string-db.org/). TNF, CASP1, MMP3, IL1B, CYP1B1, MMP13, PPARA, CNR2, and MMP9 in "Potential DEGS" are imported into lists of names to obtain the PPI protein interaction network diagram text file and import it into Cytoscape3.7.1 software. Based on the "Degree" algorithm, topological analysis of key differential genes ("critical DEGs") involved in drug-mediated NF-κB signaling pathway intervention in heart failure was performed using the Cytohubba plug-in.

Using the expression matrices of GSM8979 and GSM8982-GSM8998 in the GSE591 chip as the validation set, independent sample *t*-test analysis was performed on the expression matrix of "core DEGs" using the R language ggplot2 package to observe their expression status and draw a group comparison chart.

Using the DAVID (https://david.ncifcrf.gov/) database, the "Homo sapiens" species were selected, and data on the biological process (BP), cellular component (CC), molecular function (MF), and pathway (Kyoto encyclopedia of genes and genomes, KEGG) of "potential DEGs" were obtained. BP, CC, and MF are collectively known as gene ontology (GO). Using the R language gglopt package, the top five GO, five KEGG bubble maps, and five KEGG target pathway maps were based on - Log10 (p.adjust), p.adjust, and Count values.

To access the structural information of Hydroxysafflor yellow A, calycosin-7-O-β-D-glucoside, salvianolic acid B, calycosin, and formononetin, the PubChem database (https://pubchem.ncbi.nlm.nih.gov) was utilized. This database provided access to the chemical structures of these compounds in either primer or SDF format, available in both 2D and 3D visualizations. The structure diagram of the obtained drug is successively passed through Chem3D software, the minimum free energy is selected, the optimization is carried out, and the file is kept in mol2 format. The Alphafold database (https://alphafold.com/) was run to obtain the PDB file of path DEGs. Pymol software was introduced to optimize the water removal hydrogenation. AutodockTools software was used to sequentially dock drugs with drug-mediated NF-κB signaling pathways to intervene in heart failure differential genes ("pathways DEGs": TNF, IL1B), the binding energy was calculated, and the results were saved in a pdbqt format file. Finally, Pymol software was used to optimize the 3D structure of the molecular docking results.

Animals and Grouping

Sixty adult healthy SPF grade SD rats—weighing 200–220 g—were purchased from Hunan Slake Experimental Animal Co., Ltd. (certificate number 430727221102192317). All animals were acclimatized to laboratory conditions for three days before the experiment. The animals were placed in a standard polypropylene cage at a temperature of 23±2°C and humidity of 56% ± 4% and fed freely with water. The experiment was approved by the Animal Experiment Ethics Review Committee of Hunan University of Chinese Medicine (Number: LL2022030207). All the animal care and experimental procedures follow the Guidelines for the Care and Use of Laboratory Animals developed by the Ministry of Science and Technology of China, and the Animal Experiment Ethics Committee of the Hunan University of Chinese Medicine, and all methods are reported in accordance with ARRIVE guidelines for the reporting of animal experiments. The rat HF model was established by ligating the anterior descending branch of the rat's left coronary artery.[14] The rats were weighed and anesthetized by intraperitoneal injection of 0.26 mL/100 g of 2% pentobarbital sodium (Germany, Merck KGaA, No. P3761). The trachea was intubated and connected to an artificial ventilation machine with a respiratory rate of 80 breaths/min and a tidal volume of 7–9 mL.

After thoracotomy, needles were inserted into the coronary vein branch at the edge of the left atrial appendage, and a needle was inserted 1 mm below the pulmonary artery cone. The chest was closed swiftly and sutured after ligation of the coronary artery and vein with a 6/0 suture. In the sham surgery group, a small loop of the surgical thread was made, similar to the preceding approach without ligation. An electrocardiogram machine was connected, and the electrocardiogram showed that the ST-T segment of the chest lead was elevated, indicating successful ligation. After surgery, each rat was injected with 400,000 units of penicillin daily for three consecutive days to prevent infection. After establishing the model, the animals underwent routine disinfection for four weeks until cardiac function was measured using

echocardiography. After removing the dead and unsuccessfully modeled rats, 30 HF and six sham-operated rats were ultimately left. Thirty HF rats were randomly divided into five groups. Successfully modeled rats were divided into model, YXT low-dose (1.4 g/kg), YXT medium-dose (2.8 g/kg), YXT high-dose (5.6 g/kg), and trimetazidine groups (0.01 g/kg) based on a random number table Each group was treated by gavage, whereas the sham surgery and model groups were treated with equal amounts of distilled water. The gavage volume of each group was 10 mL/kg daily for four consecutive weeks.

Reagents and Chemicals

GAPDH (product number: GB15002), PKC-β (Product number: GB113782), NF-κB (product number GB12142), RIPA cracking liquid (product number G2002-100ML), 50 × Cocktail protease inhibitor (product number: G2006-250UL), PMSF (100 mM) (product number: G2008-1ML), BCA protein quantitative detection kit (product number: G2013), SDS-PAGE gel preparation kit (product number: G2003-50T), PVDF membrane 0.45 μm (product number: WGPVDF45), TWEEN 20 (product number: GC204002-100 mL), ECL chemiluminescence kit (product number: G2014-50ML), electron microscope fixative (product number: G1102) HE dye solution set (product number: G1003), all of which were purchased from Servicebio Company (Hubei, China). The following products were included in our study: Neutral gum (product number: 10004160, China National Pharmaceutical Group Chemical Reagent Co., Ltd.), Masson dye kit (product number: G1006, Servicebio company), differentiation solution (product number: G1039, Servicebio company); TMAO standard product (article number: 92277–10G, Sigma, USA).

The rat atrial natriuretic peptide (ANP) ELISA kit (product number: AF40118-A), rat brain natriuretic peptide/brain natriuretic peptide (BNP) ELISA kit (product number: AF2943-A), rat N-terminal proBNP ELISA kit (product number: AF3205-A), rat tumor necrosis factor α (TNF-α) ELISA kit (product Number: AF3056-A), Rat Interleukin 1β (IL-1β), ELISA kits (product number AF2923-A), and rat interleukin-6 (IL-6) ELISA kit (product number: AF3066-A) were all produced by Aifang Biotechnology Co., Ltd. (Hunan, China).

Evaluation of Echocardiographic Parameters

The cardiac function of mice treated for four weeks was evaluated using a small-animal color Doppler ultrasound imaging system (Feieno Technology Co., Ltd., model: 6LAB. China). The rats were anesthetized with isoflurane (Rayward Life Technology Co., Ltd., China). After anesthesia, the rats were fixed in a dorsal position, and a small-animal color Doppler ultrasound imaging system was used to obtain the long- and short-axis sections of the parasternal left ventricle and the papillary muscle level. The detection indicators included the left ventricular ejection fraction (EF) and left ventricular shortening fraction (FS).

Histopathological Studies

After serum testing, the rats were euthanized, and their hearts were removed. The heart was fixed in 4% paraformaldehyde for 48 h, dehydrated in a continuous solution of ethanol and xylene, and embedded in paraffin. The heart was then sliced evenly at a thickness of 5 μM. Next, the sections were stained with HE and Masson's, and the myocardial tissue was observed under NIKON DS-U3 (Japan).

Transmission Electron Microscope (TEM) Analysis

Fresh myocardial tissue was taken, with a tissue volume generally not exceeding 1×1×1 mm, and the electron microscope fixing solution was inserted at 4 °C for 2–4 h. Then, the tissues were rinsed with 0.1 M phosphate buffer phosphate buffer (PB) (PH7.4) thrice for 15 min each time. 1% osmic acid·0.1 M phosphate buffer PB (PH 7.4) was fixed at room temperature (20 °C) for 2 h.The sample was rinsed three times with 0.1 M phosphate buffer (PB) at pH 7.4, each rinse lasting 15 min. This was followed by a serial dehydration process, where the sample underwent treatment with increasing concentrations of ethyl alcohol (50%, 70%, 80%, 90%, 95%, and then 100%) for 15 min at each concentration. The process continued with a mixture of 100% ethyl alcohol and 100% acetone for 15 min, concluding with 100% acetone for another 15 min. For embedding, a ratio of acetone to 812 embedding agents of 1:12 was used for 4 h, followed by a 1:2 ratio for overnight penetration, and finally, pure 812 embedding agents were applied for 5–8 h. The pure 812 embedding

agent was poured into the embedding plate, inserted into the embedding plate, baked overnight in a 37°C oven, and then polymerized in an oven at 60°C for 48 h. Then, 60–80 nm ultra-thin sections were sliced using Leica UC7 (Leica Company). Double staining was performed with uranium and lead (2% uranium acetate saturated alcohol solution and lead citrate, each staining for 15 min), and the slices were dried overnight at room temperature. Images were collected for analysis under a transmission electron microscope (HT7700, Hitachi).

TMAO Measurement by UPLC-MS/MS

Serum TMAO levels were quantified using ultra-high-performance liquid chromatography-tandem mass spectrometry (UPLC-MS/MS) with isotope labeling. An appropriate amount of TMAO standard (Sigma Aldrich, St. Louis, MO, USA) was accurately weighed, and a 2.00 mg/mL stock solution was prepared with methanol for future use, labeled as S01. S01 was sequentially diluted with methanol into standard curve working solutions with concentration gradients of 5000, 2000, 500, 200, 20, and 2 ng/mL. The stock and standard curve working solutions were stored at −20 °C. A specific amount of the sample was accurately measured and mixed with three times its volume of methanol. This mixture was vortexed for 10 min, centrifuged at 13,000 rpm for 10 min, and the supernatant was collected for analysis. The supernatant was injected into a hydrophilic liquid chromatography normal-phase silica column for analysis (4.6×150 mm, 5μm, Waters) with the following parameters: Injection volume of 2μL, column temperature of 40°C, mobile phase of A-10 m ammonium formate water (containing 0.1% formic acid), and B-acetonitrile, as well as a flow rate of 1.0 mL/min. The gradient elution conditions used are listed in Table 2. The chromatogram collection and integration of TMAO were processed using the Xcalibur software (version 3.0; Thermo Fisher Scientific), and linear regression was performed with 1/X2 as the weighting coefficient.

Measurement of IL-1β, IL-6, TNF-α, NT-proBNP, ANP, and BNP Levels

After completing echocardiography, blood samples were collected from the abdominal aorta of the rats. Following the manufacturer's instructions, the rat atrial natriuretic peptide (ANP) ELISA kit, rat brain natriuretic peptide/brain natriuretic peptide (BNP) ELISA kit, rat N-terminal proBNP ELISA kit, rat tumor necrosis factor α (TNF-α) ELISA kit, rat interleukin 1β (IL-1β) ELISA kit, and rat interleukin-6 (IL-6) ELISA kit were used.

RT-qPCR

After removing the myocardial tissue, total RNA was extracted from the homogenized myocardial tissue using an RNA extraction solution (Servicebio, China). The concentration and purity of total RNA were determined using a nucleic acid/protein analyzer (Thermo, USA). Subsequently, according to the manufacturer's instructions, cDNA was synthesized using a reverse transcription kit (Servicebio, China). RT-qPCR analysis was performed using the SYBR Green RT-qPCR kit (Servicebio, China) and the CFX Connect real-time PCR system (Bio radUSA) according to the manufacturer's instructions. The relative expression levels of the respective mRNAs were quantified using the $2^{-\Delta\Delta Ct}$ method with GAPDH as an endogenous reference, and the primer sequences are shown in Table 3.

Table 2 Chromatographic Gradient

Time (min)	Phase A	Phase B
0.00	95	5
1.00	95	5
2.50	10	90
3.50	10	90
3.80	95	5
5.00	95	5

Table 3 Primer Sequences for Real-Time PCR

Target Gene		Primer Sequence(5'to3')
PKC	Forward	TAGGGAAAGGCAGTTTTGGG
PKC	Reverse	TGGGAAGCCCCTGTTCTGTA
NF kB-P65	Forward	ACGATCTGTTTCCCCTCATC
NF kB-P65	Reverse	TGCTTCTCTCCCCAGGAATA
GAPDH	Forward	CGTATCGGACGCCTGGTT
GAPDH	Reverse	AGGTCAATGAAGGGGTCGTT

Western Blot Analysis

RIPA lysis buffer containing phosphatase and protease inhibitors was used to lyse the myocardial tissue, which was then placed in an ice bath for 15 min. Centrifugation was performed at 4 °C and 16,000 rpm for 15 min to extract some cytoplasmic proteins. The undiluted protein solution and protein concentrations were measured using a BCA protein concentration assay kit (Servicebio, China). Next, 20 μg of protein was loaded onto a 12% SDS-PAGE gel and transferred to a PVDF membrane (Servicebio, China). After sealing with 5% skim milk for 2 h, the PVDF membrane was washed with TBST and incubated overnight with the primary antibodies (GAPDH, PKC-β, and NF-κB p65) at 4 °C. On the second day, the membrane was washed thrice with TBST and incubated with HRP-labeled secondary antibody at 37 °C for 1 h. Finally, a highly sensitive ECL chemiluminescence substrate (Servicebio, China) was used to display protein expression, and data analysis was performed using AIWBwellTM (Servicebio, China) analysis software.

Statistical Analysis

GraphPad Prism 9 software was used to conduct statistical analysis and draw statistical charts. The experimental data are expressed as mean±SD. Single-factor analysis of variance was used to evaluate differences between multiple groups, followed by the LSD test (when variance is uniform) or Dunnett's T3 test (when variance is uneven). Differences were considered highly significant at $P<0.01$ or $P<0.05$ has statistical significance.

Results

HPLC of YXT

The chemical components of the compound formulations were identified using high-performance liquid chromatography fingerprint. Methodological investigation was conducted based on the relative peak area of the test sample chromatogram and the relative retention time (using salvianolic acid B as a reference). The results of the precision, stability, and repeatability experiments are presented in Table 4. The results show that the RSD of the precision experiments was less than 1%, indicating good precision of the instrument. Stability studies showed that the test solution could be held for 48 h with an RSD of less than 3%. The fingerprinting approach has strong repeatability because the RSD of the repeatability experiment is less than 3%. In the "Similarity Evaluation System for Traditional Chinese Medicine Chromatographic Fingerprint (2012 Edition)", 32 peaks with good separation and relatively high content were selected as the common characteristic peaks of YXT Granules' fingerprint (Figure 1A). After identification using the reference substance, the 13th peak was hydroxysafflower flavin A, the 18th peak was hairy pistil isoflavone glucoside, the 24th peak was salvianolic acid B, and the 26th peak was hairy pistil isoflavone. The 31st peak was observed for mangiferin (Figure 1B). Through matching, the fingerprint patterns of ten batches of YXT granules are shown in Figure 1C.

Table 4 Methodological Review Results

	Precision	Stability	Repeatability
Relative peak area RSD	0.54%	2.95%	2.80%
Relative retention time (RSD)	0.07%	0.06%	0.07%

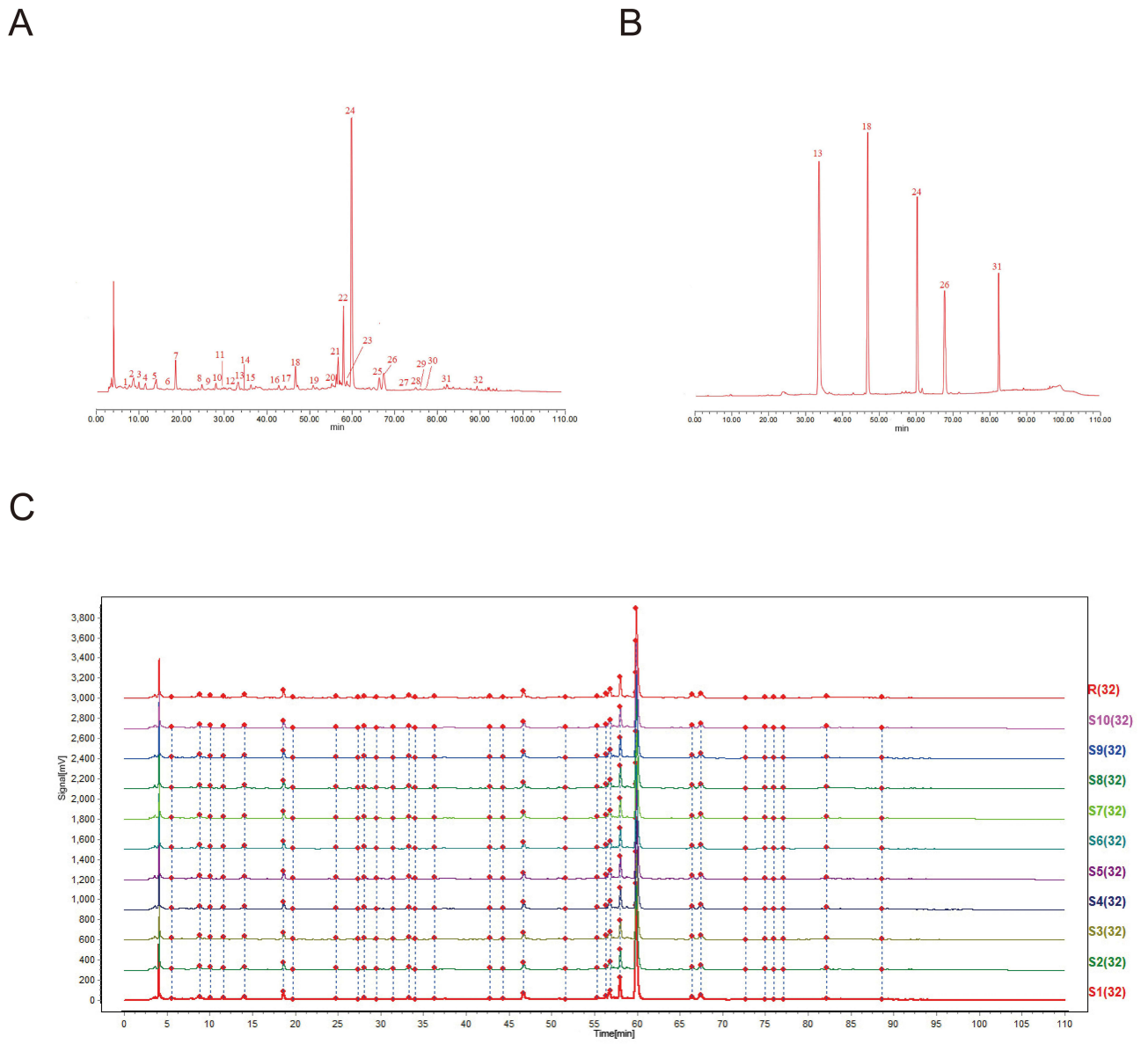

Figure 1 HPLC of YXT Granules. (**A**) HPLC of YXT Granules test sample; (**B**) HPLC of YXT Granules mixed reference substance; (**C**) Ten batches of YXT fingerprint overlay (S1-S10) and control fingerprint (R).

The similarity of ten batches of Yixintai granules is shown in Table 5. The similarity of the ten batches of Yixintai granules was above 0.97, indicating a small difference in the types contained in the characteristic spectra among the ten batches of finished products, with a high degree of consistency. This also indirectly indicates that the quality of each batch of YXT granules was stable

Network Pharmacology Analysis

Active Compounds and Targets of YXT and Targets of HF

Combined with the PubChem and Swiss Target Prediction databases, three effective targets of hydroxysafflor yellow A were obtained. There were 19 effective targets for calycosin-7-O-β-D-glucoside, 28 effective targets for salvianolic acid B, 52 effective targets for calycosin, and 56 effective targets for formonone. A total of 107 effective targets were obtained by combining the compound targets and eliminating duplicate values.

Table 5 Similarity Results

Number	S1	S2	S3	S4	S5	S6	S7	S8	S9	S10	R
S1	1.000	0.999	1.000	0.982	0.981	0.979	0.982	0.979	0.988	0.988	0.993
S2	0.999	1.000	0.999	0.981	0.980	0.979	0.981	0.978	0.987	0.987	0.992
S3	1.000	0.999	1.000	0.982	0.981	0.979	0.983	0.979	0.988	0.988	0.993
S4	0.982	0.981	0.982	1.000	0.999	0.998	1.000	0.999	0.992	0.990	0.997
S5	0.981	0.980	0.981	0.999	1.000	0.998	0.999	0.998	0.992	0.988	0.996
S6	0.979	0.979	0.979	0.998	0.998	1.000	0.998	0.998	0.990	0.989	0.996
S7	0.982	0.981	0.983	1.000	0.999	0.998	1.000	0.999	0.992	0.990	0.997
S8	0.979	0.978	0.979	0.999	0.998	0.998	0.999	1.000	0.990	0.989	0.996
S9	0.988	0.987	0.988	0.992	0.992	0.990	0.992	0.990	1.000	0.995	0.996
S10	0.988	0.987	0.988	0.990	0.988	0.989	0.990	0.989	0.995	1.000	0.995
R	0.993	0.992	0.993	0.997	0.996	0.996	0.997	0.996	0.996	0.995	1.000

A total of 1463 DEGs were obtained using the GSE591 chip, among which 898 DEGs were highly expressed in the sample matrix, and 565 DEGs were expressed at low levels in the sample matrix (Figure 2A). The heatmap shows the expression of the top 30 DEGs in the GSM8979 and GSM8982-GSM8998 samples. The red matrix shows high expression (logFC≥1), whereas the blue matrix shows low expression (logFC≤–1) (Figure 2B). The data from the standardized box diagram are shown in Table 6 and Figure 2C, and the PCA diagram shows the distribution of the samples (Table 7, Figure 2D).

Network Analysis of YXT-HF Targets

The results of Wayne diagram showed that nine "potential DEGs" were obtained, including TNF, CASP1, MMP3, IL1B, CYP1B1, MMP13, PPARA, CNR2, and MMP9 (Figure 3). It has been suggested that it can interfere with HF occurrence and development.

Two non-interacting genes (CASP1 and CNR2) were deleted from the STRING database. Topological analysis showed the interaction network diagram of five "core DEGs" genes, which were successively TNF, IL1B, MMP9, MMP3, and MMP13 according to the Degree value (Figure 4).

Result of "Core DEGs" Differential Grouping Comparison Chart

The results showed that in "key DEGs" (Table 8), IL1B, TNF, MMP3, MMP9, and MMP13 were all highly expressed in HF (Figure 5), with statistically significant differences ($P<0.001$). Preliminary results indicated that calycosin, calycosin-7-O-β-D-glucoside, formononetin, hydroxysafflor yellow A, and salvianolic acid B can mediate the PKC signaling pathway to downregulate the expression of key DEGs and thus play a role in alleviating HF.

GO and KEGG Enrichment Analysis of YXT-HF Targets

GO analysis yielded a total of 1727 entries, of which 1138 were BP entries, 5 CC entries, and 42 MF entries (Figure 6). "Potential DEGs" mainly play biological functions, such as the regulation of inflammatory response, response to peptides, regulation of neuroinflammatory response, response to amyloid beta, and neuroinflammatory response. They were also associated with molecular functions, including metal endopeptidase activity, endopeptidase activity, serine endopeptidase activity, metal peptidase activity, and serine-type peptidase activity. It was enriched in the peptidase inhibitor complex, inflammatory body complex, phagocytic cell cup, neuronal cell body, tertiary granular cavity, and other cell components (Figure 6A).

KEGG enriched 56 items that were mainly involved in the IL-17 signaling pathway, lipid and atherosclerosis signaling pathway, TNF signaling pathway, Legionnaires' disease signaling pathway, NF-κB signaling pathway, and other signaling pathways (Figure 6B and C). This study focused on the intervention of the drug-mediated NF-κB signaling pathway in HF. KEGG analysis further confirmed that "latent DEGs" can participate in the NF-κB signaling pathway to intervene in HF. Among them, the differential genes that mediate the NF-κB signaling pathway to intervene

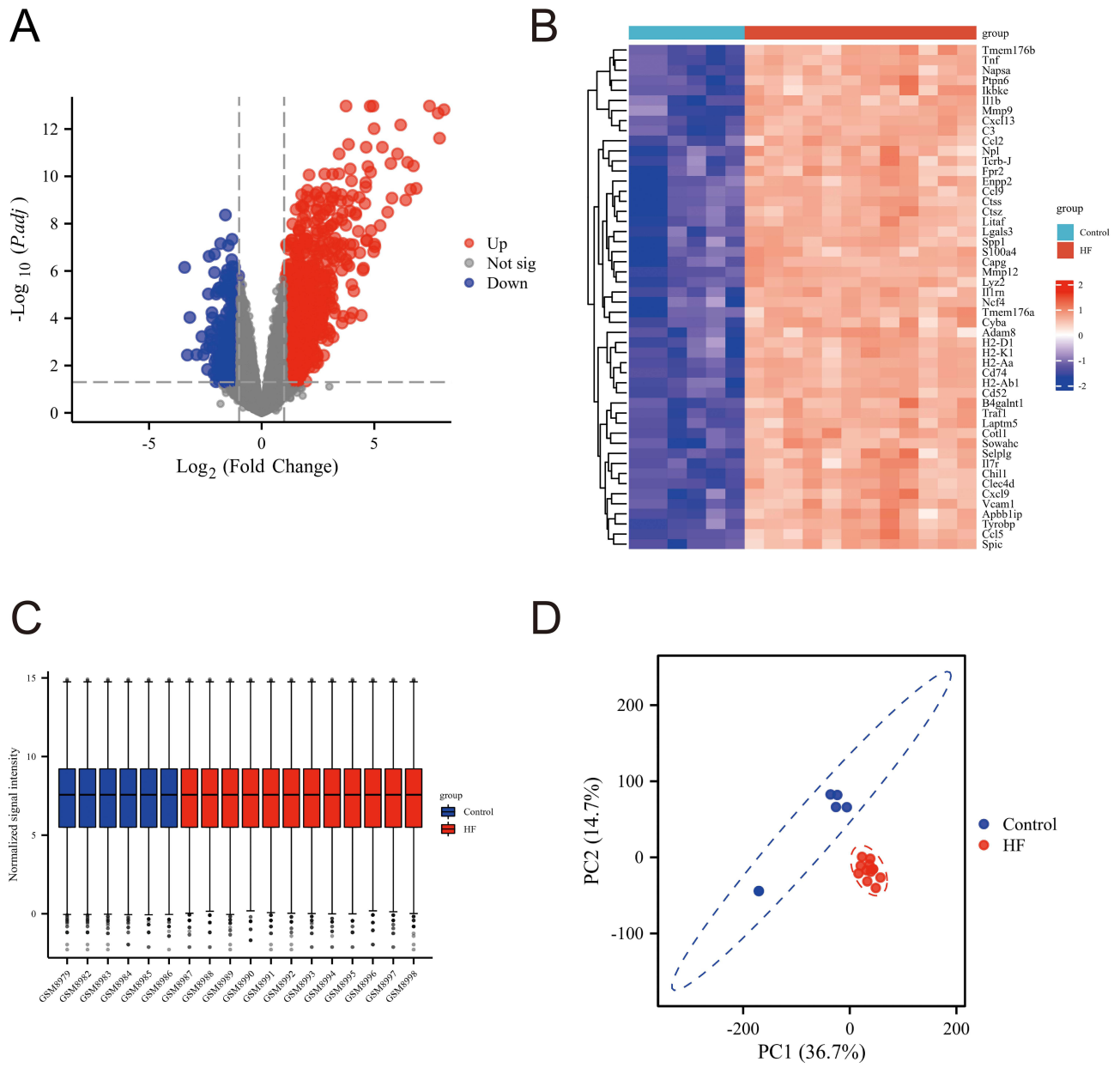

Figure 2 Differential analysis of heart failure. The DEGs are represented as a volcano figure (**A**), heatmap (**B**), Box plot (**C**) and PCA score plot (**D**) comparing the control and HF groups.

in HF are TNF and IL1B (pathway DEGs), and TNF and IL1B are the key genes in topological analysis, which supports the above studies.

Molecular Docking Results

In this study, AutodockTools software was used to conduct molecular docking between drugs and "pathway DEGS" (IL1B and TNF) to clarify their binding ability (Table 9). The results showed that the binding energies of IL1B and the drugs were all < 0 kcal/mol, suggesting that IL1B and the drugs were closely docked through an exothermic reaction under natural conditions (binding energies < 0 kcal/mol). TNF can be closely bonded with the drug hydroxysafflor yellow A, calycosin-7-o-β-D-glucoside, calycosin, and formononetin under natural conditions for thermal reactions (binding energy < 0 kcal/mol). Salvianolic acid B was not closely docked by an endothermic reaction under natural conditions (binding energy > 0 kcal/mol).

Table 6 Box Plot Analysis Data

Sample	Minimum value	Lower quartile	Average value	Upper quartile	Maximum value
GSM8979	−2.2799899	5.50309392	7.56774673	9.21311149	14.9095382
GSM8982	−2.2799899	5.50309392	7.56774673	9.21311149	14.9095382
GSM8983	−2.2799899	5.50277244	7.56700407	9.21311149	14.9095382
GSM8984	−1.95696867	5.50435213	7.56678718	9.21311149	14.9095382
GSM8985	−2.11847928	5.50245096	7.56700407	9.21311149	14.9095382
GSM8986	−2.2799899	5.50351685	7.56726695	9.21316887	14.9095382
GSM8987	−2.11847928	5.50277244	7.56701804	9.21311149	14.9095382
GSM8988	−2.11847928	5.50320122	7.56678718	9.2132374	14.9095382
GSM8989	−2.2799899	5.50309392	7.56700407	9.21311149	14.9095382
GSM8990	−1.68681264	5.50301366	7.56700407	9.21298558	14.9095382
GSM8991	−2.2799899	5.50405141	7.56710561	9.21348921	14.9095382
GSM8992	−2.2799899	5.50091288	7.56700407	9.21311149	14.9095382
GSM8993	−2.11847928	5.50309392	7.56697416	9.2132374	14.9095382
GSM8994	−2.11847928	5.50309392	7.56700407	9.21311149	14.9095382
GSM8995	−2.11847928	5.50330852	7.56700407	9.21311149	14.9095382
GSM8996	−1.95696867	5.50367996	7.56774673	9.21311149	14.9095382
GSM8997	−2.11847928	5.50316591	7.56713551	9.21281252	14.9095382
GSM8998	−2.2799899	5.50277244	7.56700407	9.2132374	14.9095382

Table 7 PCA Distribution of Different Samples

Data Set	Sample	Grouping	PCA (Control)	PCA (HF)
GSE591	GSM8979	Control	−170.615565	−44.2857697
GSE591	GSM8982	Control	−170.615565	−44.2857697
GSE591	GSM8983	Control	−36.043379	82.6697698
GSE591	GSM8984	Control	−25.972999	66.1209363
GSE591	GSM8985	Control	−5.53507769	65.8829021
GSE591	GSM8986	Control	−23.3826054	81.9476973
GSE591	GSM8987	HF	31.4628348	−16.983423
GSE591	GSM8988	HF	43.6284042	−15.5761078
GSE591	GSM8989	HF	20.3913466	−11.0858426
GSE591	GSM8990	HF	43.7152642	−15.4298959
GSE591	GSM8991	HF	22.925609	0.66472547
GSE591	GSM8992	HF	36.7093321	−9.40800035
GSE591	GSM8993	HF	32.892598	−31.5821408
GSE591	GSM8994	HF	57.530902	−26.5895514
GSE591	GSM8995	HF	48.8066476	−40.2285395
GSE591	GSM8996	HF	38.4397193	−1.76799805
GSE591	GSM8997	HF	39.4063065	−18.9203592
GSE591	GSM8998	HF	16.2562266	−21.1426331

3D visualization using PyMOL software (Figure 7) showed that the "pathway DEGs" can form hydrogen bonds with drugs. For example, hydroxysafflor yellow A can form a hydrogen bond with amino acids at positions 18, 20, and 22 of TNF (ie, proline, lysine, and glycine).

It was further confirmed that TNF and IL1B of pathway DEGs could be hydroxysafflor yellow A, calycosin-7-O-β-D-glucoside, and salvianolic acid B. The combination of salvianolic acid B, calycosin, and formononetin regulates the NF-κB signaling pathway to intervene in HF.

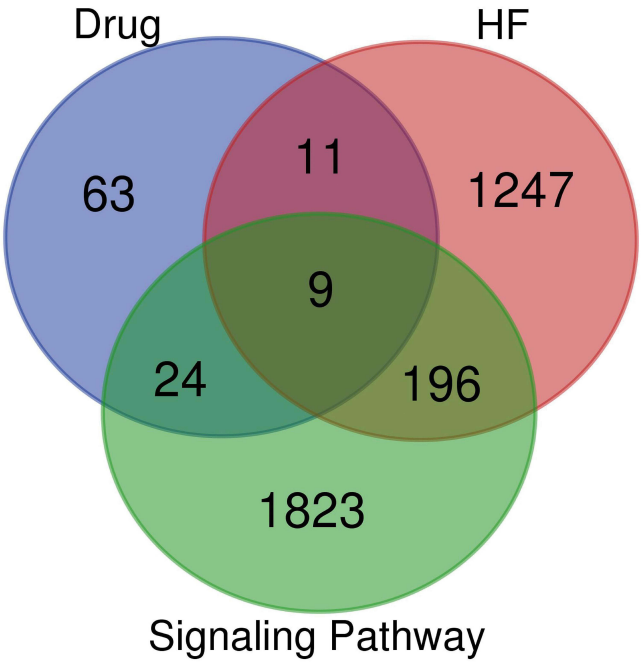

Figure 3 YXT intervenes in "potential DEGs" of heart failure.

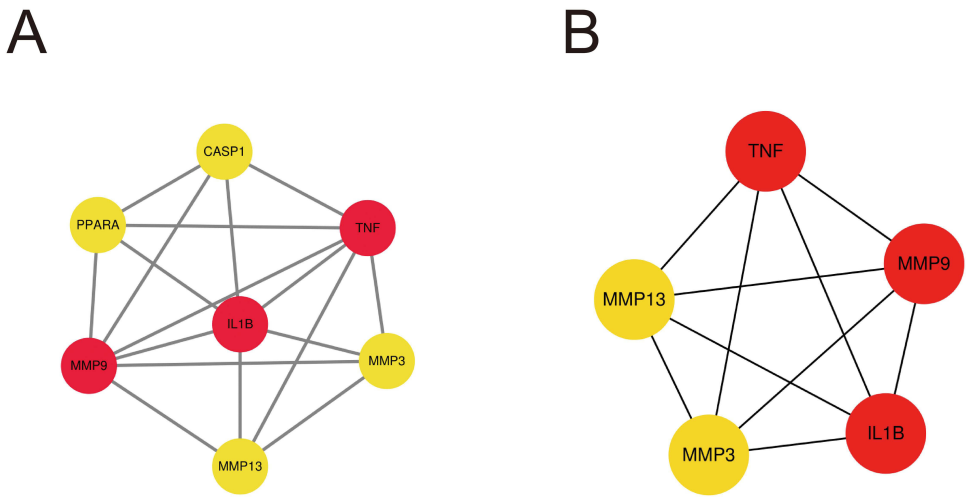

Figure 4 Core DEGs PPI topology analysis.A:The PPI network used Cityscape 3.7.1 software for visual analysis. (**B**) PPI network of more significant proteins extracted from (**A**) by filtering 2 parameters: CASP1, CNR2.The redder the target color, the larger the degree, and the yellower the color, the smaller the degree.

Effect of YXT on Heart Function

Echocardiography was used to test whether YXT improves cardiac function in rats with AMI-induced HF (Figure 8A). Compared with the sham surgery group, EF and FS values of the model group were significantly lower than those of the sham decrease ($P<0.01$). Compared with the model group, the low-, medium-, and high-dose YXT and trimetazidine groups showed a significant increase in cardiac ultrasound EF and FS values ($P<0.01$), as shown in Figure 8B. According to the echocardiography results, YXT can improve the cardiac function in rats with AMI-induced HF.

Effect of YXT on Cardiac Fibrosis in HF Rats

To investigate whether YXT can improve the morphology of myocardial cells and the degree of myocardial fibrosis in AMI-induced HF in rats, we used HE staining to observe myocardial cell morphology, while Masson staining showed the

Table 8 "Core DEGs" Expression Matrix Data

Sample	IL1B	TNF	MMP3	MMP9	MMP13
GSM8979	5.264625	6.177688	6.213373	6.561734	4.578397
GSM8982	5.264625	6.177688	6.213373	6.561734	4.578397
GSM8983	3.798339	4.905139	3.98137	3.850469	6.435413
GSM8984	3.057414	4.787309	5.299465	3.826618	6.377765
GSM8985	4.466382	4.001312	5.628867	3.626485	6.441895
GSM8986	4.450132	4.863526	5.595517	3.735488	6.113966
GSM8987	9.085869	12.95737	7.64221	11.67136	5.375279
GSM8988	8.756862	13.66446	8.452521	11.76371	4.190298
GSM8989	8.99559	12.96197	8.131753	11.22921	3.086841
GSM8990	8.306903	12.52855	5.756839	11.22567	4.201295
GSM8991	8.872325	12.85916	6.060473	11.43758	4.402582
GSM8992	8.725688	13.56216	5.720254	11.64592	5.040514
GSM8993	8.105747	13.45065	5.628867	11.34089	5.720945
GSM8994	8.653881	13.31917	6.341135	11.30589	4.48997
GSM8995	8.174965	13.75011	6.090154	11.44303	5.022494
GSM8996	9.080188	13.24723	7.229046	11.71302	4.905139
GSM8997	8.870753	13.21636	8.669432	12.08948	5.246784
GSM8998	9.005727	13.44372	8.18409	11.78928	4.632151

degree of myocardial fibrosis, myocyte morphology and myocardial fibrosis. In HE staining, the nucleus was blue, and the cytoplasm was red. The collagen fibers showed a blue color on Masson's staining. The muscle fibers, cellulose, and red blood cells are red. The sham surgery group had a normal tissue structure, cleanly distributed myocardial cells, and evident transverse stripes. No inflammatory cell infiltration was observed between tissues. Compared with the normal group, most myocardial fibers in the model group showed autolysis, with muscle fiber breaking, curling, and disorderly arrangement. The myocardial cell nucleus was significantly pyknotic, ruptured, and disappeared. Most cells and myocardial bundles under the pericardium were infiltrated by lymphocytes and macrophages. Compared with the model group, the low-dose YXT group showed atrophy and thinning of myocardial fibers, with autolysis and poor alignment. The muscle fibers of the YXT medium-dose group were arranged neatly, with many lymphocytes and macrophages still infiltrating, a small amount of myocardial cell nucleus pyknosis, and visible rupture and disappearance of myocardial cells. In the high-dose group of YXT, most muscle fibers were arranged clearly and neatly, with only a small amount of lymphocyte infiltration and a small portion of myocardial cell nuclei pyknosis without rupture or disappearance. The muscle fibers in the trimetazidine group were arranged in an orderly manner, with a small number of infiltrating lymphocytes and macrophages, no obvious myocardial cell nucleus pyknosis, and no rupture or disappearance.In the normal group, except for the large blood vessels in the heart, normal inner and outer membranes, and a small amount of fibrous tissue hyperplasia in the myocardium, no fibrous tissue hyperplasia was observed. Compared with the sham surgery group, the blue staining area of cardiac collagen fibers in the model group mice was significantly increased. Compared with the model group, the blue staining area of cardiac collagen fibers in the low-, medium-, and high-dose YXT groups gradually decreased in a dose-dependent manner. The blue staining area of the cardiac collagen fibers in the trimetazidine group was the smallest (Figure 9).

Effect of YXT on Mitochondrial Ultrastructure

We used TEM to analyze the mitochondrial ultrastructure of rats with HF. In the sham-operated group, the rat myocardial mitochondria were arranged regularly, with uniform volume, no swelling or deformation, clear and complete cristae, neatly arranged sarcomeres, and intact structures in all parts. The myocardial mitochondria in the model group were enlarged and hypertrophic, with variable forms, damaged cristae, and disordered muscle fibers. The low-dose YXT group showed swelling and deformation of the mitochondria, increased volume, blurred mitochondrial cristae, and unclear sarcomere display. The moderate dose group of YXT showed partial myocardial mitochondrial edema and uneven

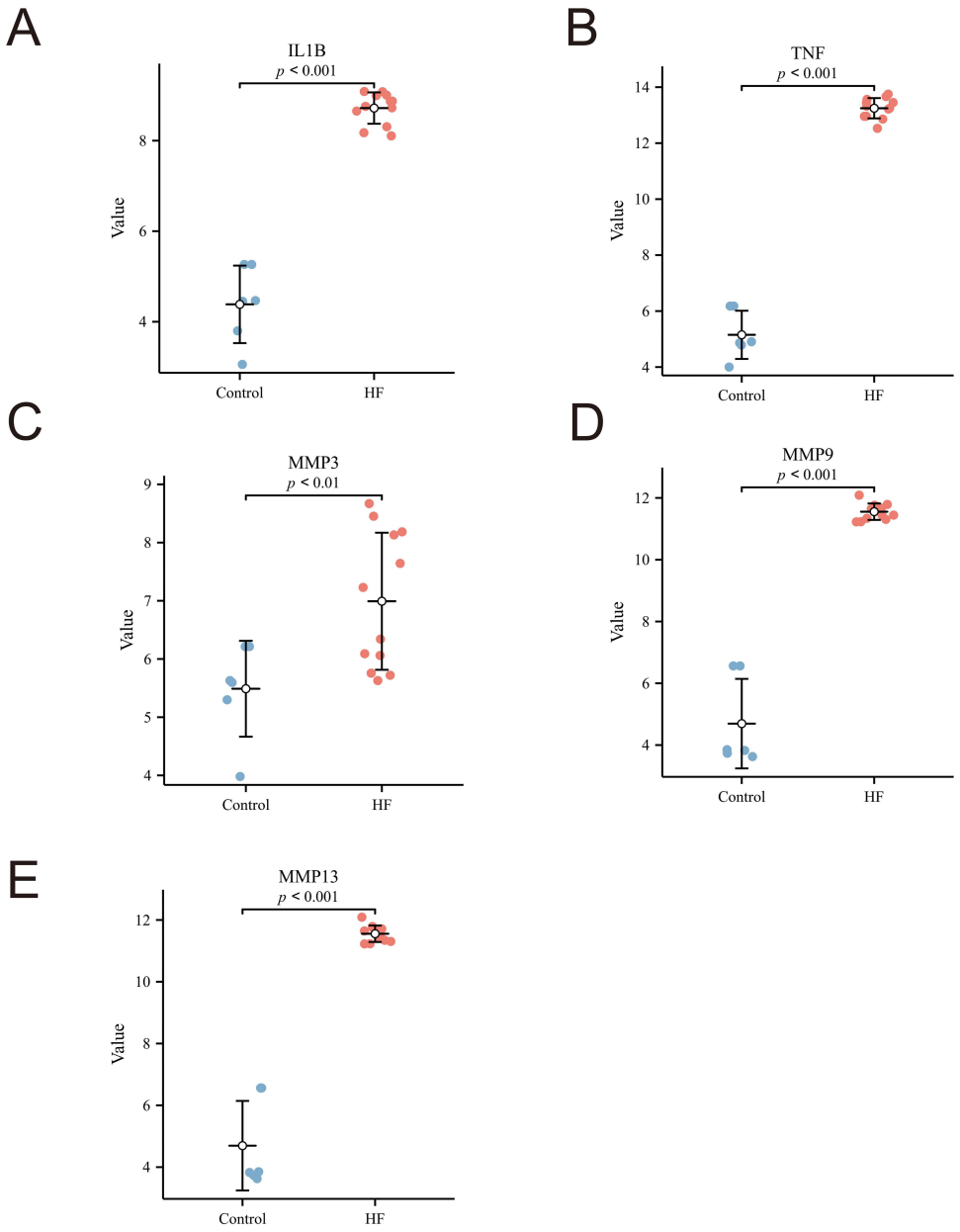

Figure 5 "Core DEGs" Difference Group Comparison Chart. (**A**) IL-1β; (**B**) TNF-α; (**C**) MMP3; (**D**) MMP9; € MMP13.

morphology, milder than the model group, with slightly disordered cristae and relatively neat sarcomeres. The high-dose group of YXT showed a relatively neat arrangement of myocardial mitochondria, mild edema, and deformation; some cristae were blurry, the sarcomere arrangement was relatively neat, and the degree of morphological changes was lighter than in other medication groups. The mitochondria in the trimetazidine group were arranged neatly, with mild edema and deformation; some cristae were blurry, sarcomeres were arranged neatly, and the degree of morphological changes was lighter than that in other medication groups (Figure 10).

Effect of YXT on NT-proBNP, ANP, BNP and Inflammatory Factor Indicators in Rats

We used ELISA to measure NT-proBNP, ANP, and BNP levels in rat serum. Compared with the sham surgery group, the serum NT-proBNP, BNP, and ANP levels in the model group were significantly increased (P<0.01). Compared with the

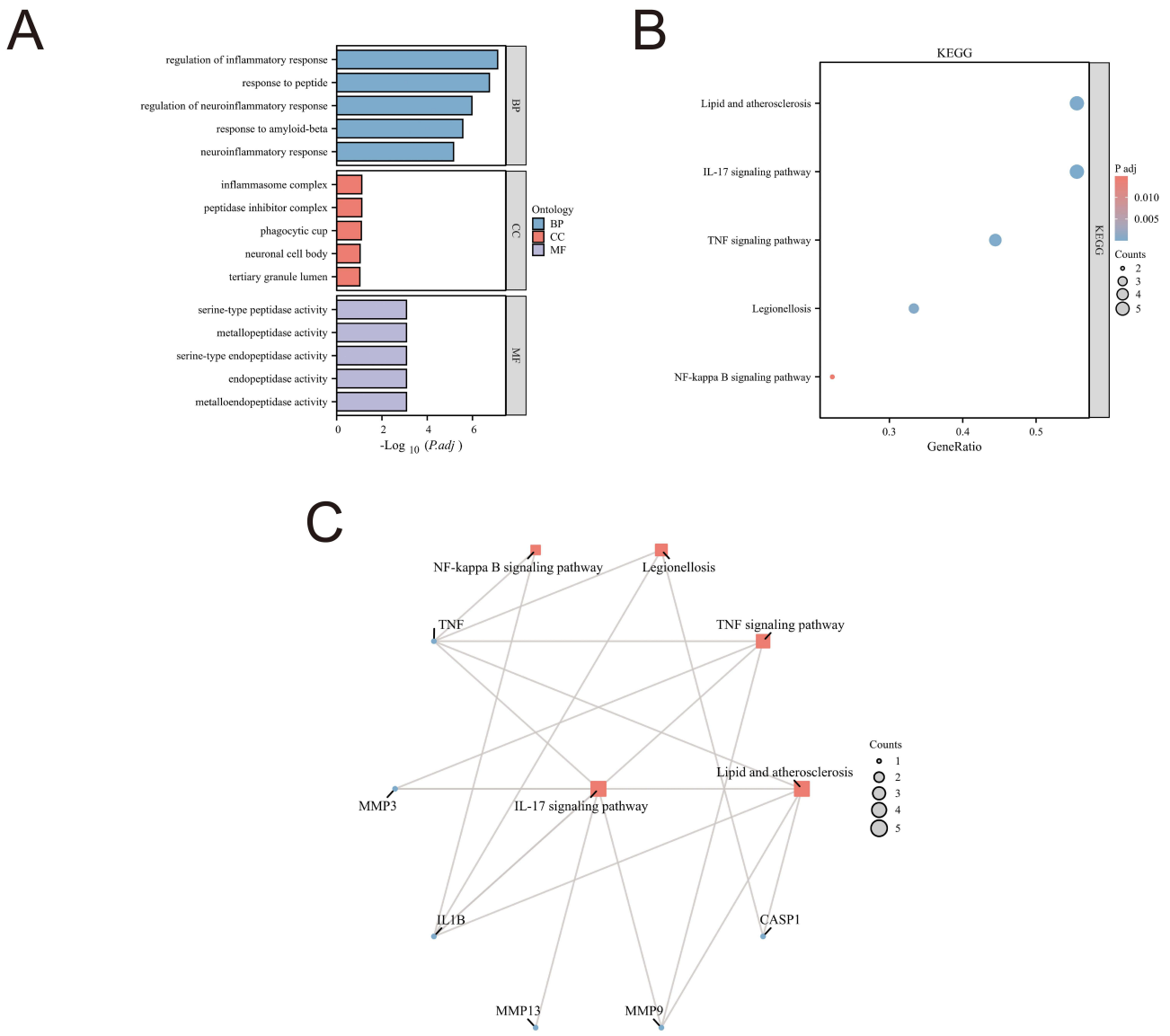

Figure 6 Potential gene GO and KEGG analysis; (**A**) GO analysis; (**B**) KEGG analysis; (**C**) KEGG target pathway diagram.

model group, the serum NT pro-BNP, BNP, and ANP levels in the middle dose, high dose, and trimetazidine groups of YXT granules were significantly reduced (P<0.01; Figure 11A–C). YXT can improve heart function in HF rats.

We used ELISA to quantify serum levels of IL-1β, IL-6, TNF-α, and other inflammatory factors to assess the effectiveness of YXT in improving inflammation in rats with AMI-induced HF. The model group exhibited significantly higher serum levels of IL-1β, IL-6, and TNF-α than the sham surgery group (P<0.01; Figure 11D–F). The medium and high groups of YXT granules and trimetazidine group showed significant decreases in serum IL-1β, IL-6, and TNF-α compared to the model group (P<0.05; Figure 11D–F).

Effect of YXT on Serum TMAO in Rats

We measured the serum TMAO levels of the rats in each group. Compared with the sham surgery group, the model group showed a significant increase in serum TMAO levels (P<0.01; Figure 12). Compared with the model group, the low-, medium-, and high-dose groups of YXT granules and the trimetazidine group showed a decrease in serum TMAO (P<0.01; Figure 12). The results showed that serum TMAO content in rats with HF was greatly increased, while YXT reduced it.

Table 9 Binding Energy Data of "Pathway DEGs" and "Drug" Docking

Active Ingredient	Core DEGs	Binding Energy
hydroxysafflor yellow A	TNF	−0.37kcal/mol
Calycosin-7-O-β-D-glucoside	TNF	−3.37 kcal/mol
Salvianolic Acid B	TNF	1.05 kcal/mol
Calycosin	TNF	−5.73 kcal/mol
Formononetin	TNF	−6.83 kcal/mol
hydroxysafflor yellow A	IL-1β	−4.41 kcal/mol
Calycosin-7-O-β-D-glucoside	IL-1β	−7.17 kcal/mol
Salvianolic Acid B	IL-1β	−6.6 kcal/mol
Calycosin	IL-1β	−5.28 kcal/mol
Formononetin	IL-1β	−5.57 kcal/mol

Effect of YXT on PKC/NF-κB Pathway

Based on the results of the network pharmacology analysis, we further validated the involvement of the TMAO/PKC/NF-κB signaling pathway in myocardial hypertrophy after YXT treatment. Western blotting and RT-qPCR results indicated that compared with the sham surgery group, the model group showed a significant increase in PKC and NF-κB p65 mRNA expression in myocardial tissue (P<0.01; Figure 13A and B). The low-, medium-, and high-dose YXT and trimetazidine groups showed significantly reduced PKC and NF-κB p65 mRNA expression in myocardial tissue compared with the model group (P<0.01; Figure 13A and B). Compared with the sham surgery group, NF-κB and PKC protein expression in the myocardial tissue of the model group was significantly increased (P<0.01; Figure 13C–E). Compared with the model group, TMAO, NF-κB, and PKC expression in myocardial tissue was reduced in the low-, medium-, and high-dose groups of YXT and trimetazidine group (P<0.01; Figure 13C–E). These data indicate that the TMAO/PKC/NF-κB signaling pathway is activated in the myocardium of rats with heart failure, while YXT inhibits the signaling pathway.

Discussion

HF is the late stage of most chronic cardiovascular diseases, with a poor prognosis, high hospitalization rate, and high mortality rate, burdening patients' families and society. Combining the advantages of TCM with modern medicine is of

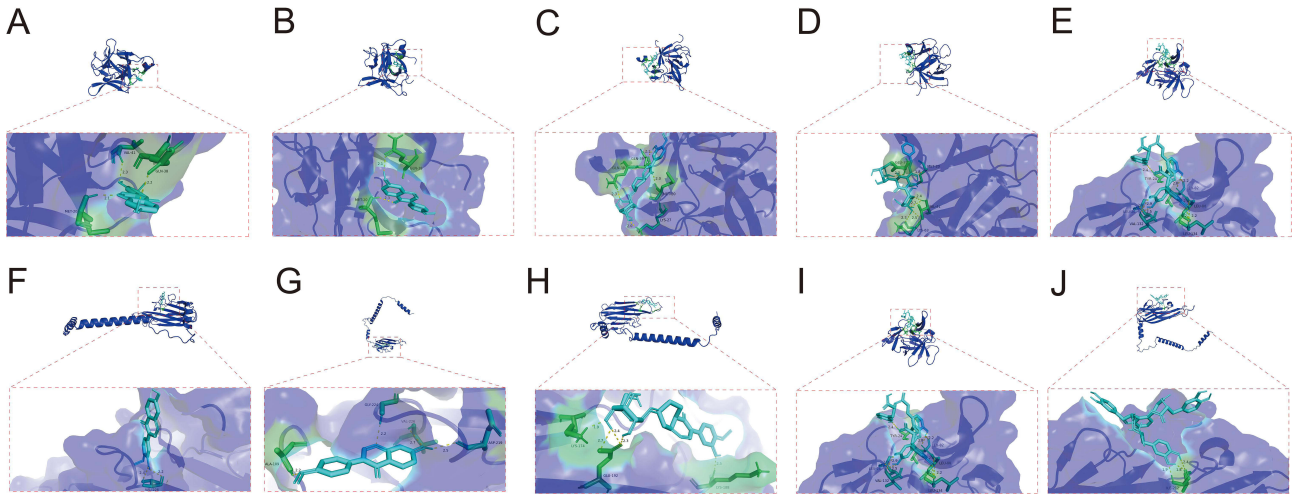

Figure 7 Visualization of the interface between Core DEGs and Active Ingredients: (**A**) Result of docking IL1B with Calycosin; (**B**) Result of docking IL1B with Formononetin. (**C**) Result of docking IL1B with Calycosin-7-O-β-D-glucoside; (**D**) Result of docking IL1B with hydroxysafflor yellow A; (**E**) Result of docking IL1B with Salvianolic Acid B; (**F**) Results of docking between TNF and Calycosin; (**G**) Results of the docking between TNF and Formononetin; (**H**) The docking result of TNF and Calycosin-7-O-β-D-glucoside; (**I**) The docking result of TNF and hydroxysafflor yellow A; (**J**) The docking result of TNF and Salvianolic Acid B.

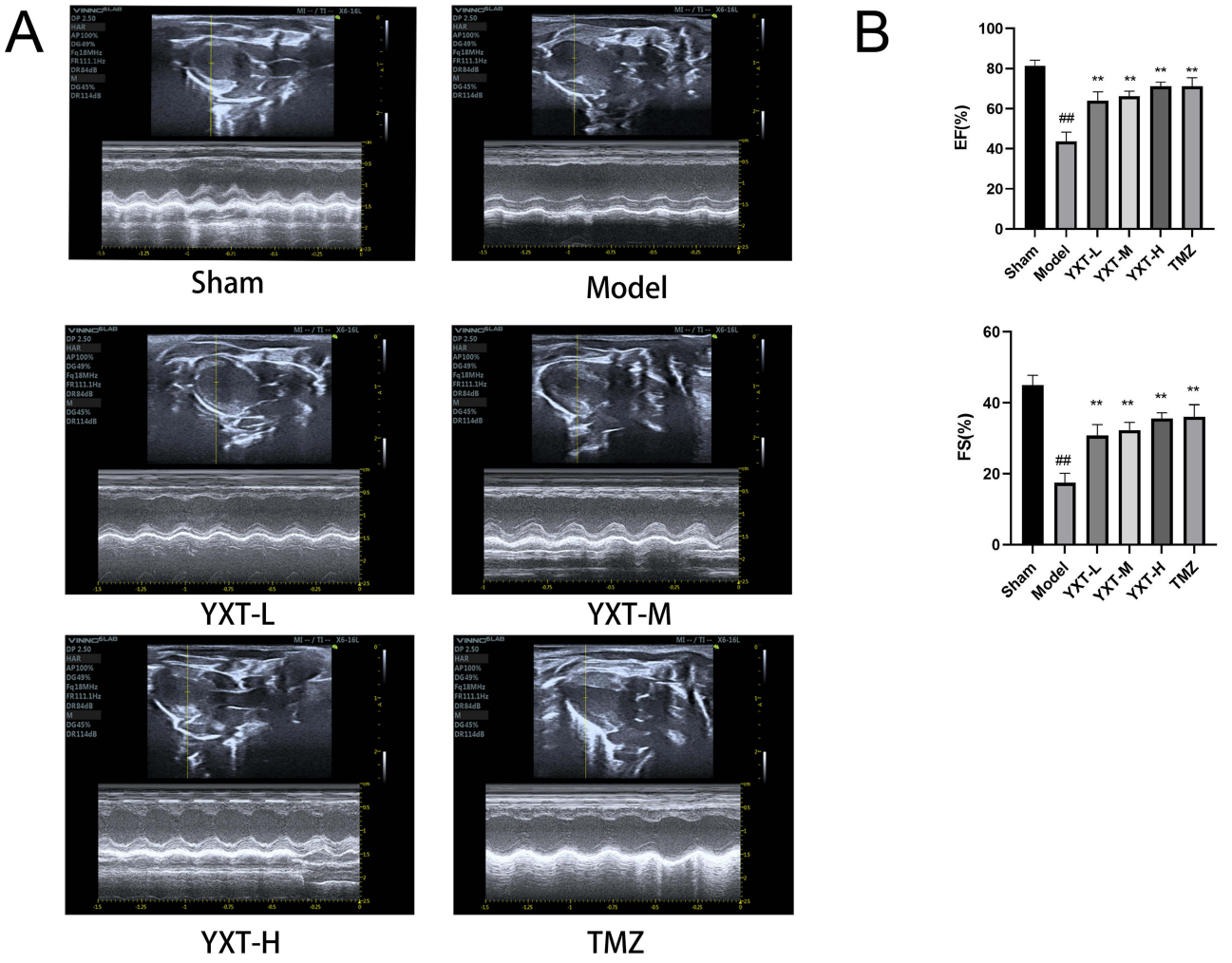

Figure 8 Cardiac ultrasound results of rats in each group. (**A**) Cardiac global function was quantitatively assessed from two-dimensional echocardiographic short axis images among the different groups; (**B**) Cardiac systolic function was determined by measuring ejection fraction (EF) and fraction shortening (FS).n=6. $^{\#\#}P<0.01$ vs sham group; $^{**}P<0.01$ vs model group; All values are depicted as mean ± SD.

great significance for diagnosing and treating chronic HF. Recent evidence suggests the potential significance of the gut microbiota and its metabolites in mediating or regulating HF pathophysiology.[15] The gut microbiota can influence HF occurrence and development by producing metabolites, such as short-chain fatty acids, bile acids, and TMAO. Specifically, TMAO can increase the risk of HF, affect the prognosis of HF, and reduce the long-term survival rate of patients with HF.[16] TMAO can trigger heart failure by affecting myocardial hypertrophy and fibrosis, inducing inflammatory responses, and exacerbating mitochondrial dysfunction.[6] Therefore, TMAO is an important therapeutic target in HF treatment.

YXT is a classic clinical prescription containing multiple classic Chinese herbal medicine pairs. Astragalus membranaceus (Fisch.) Bunge and Panax ginseng C. A. Mey are classic Qi tonifying drug pairs. Ginsenoside Rd promotes mitochondrial biosynthesis and improves myocardial cell damage during heart failure.[17] Astragalus membranaceus (Fisch.) Bunge can improve heart function by regulating heart failure metabolites.[18] Salvia miltiorrhiza Bunge and Carthamus tinctorius L. are classic pairs of blood-activating and stasis-resolving drugs, respectively. Danshen injection (a TCM extracted from Salvia miltiorrhiza Bunge) can significantly prevent myocardial fibrosis, hypertrophy, hemodynamic deterioration, and systolic and diastolic dysfunction in patients with HF.[19] Carthamus tinctorius L. can improve lipopolysaccharide-induced myocardial cell fibrosis.[20] Poria cocos(Schw) Wol, Polyporus umbellatus (Pers.) Fr., Alisma plantago-aquatica L., and Draba nemorosa L. are classic diuretic and moisturizing drug combinations. TCM

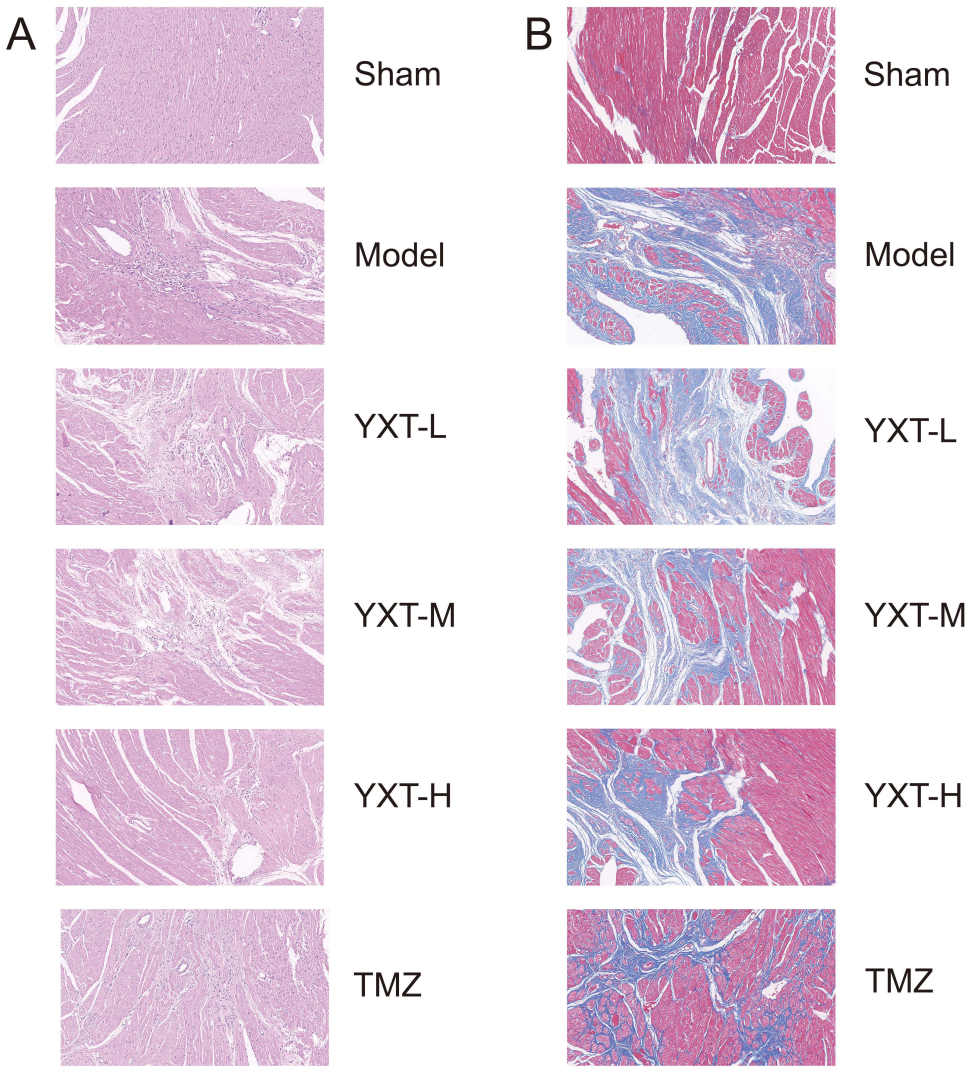

Figure 9 HE and Masson staining images of rat hearts in each group (× 200). (**A**) HE staining images; (**B**) Masson staining images.

combination of Poria cocos(Schw) Wol, Polyporus umbellatus (Pers.) Fr. and Alisma plantago-aquatica L. is derived from the formula Wuling San in Zhang Zhongjing's "Treatise on Febrile Diseases", compiled during the Han Dynasty. Poria cocos(Schw) Wol can improve heart function in congestive heart failure rats,[21] and the aqueous extract of Polyporus umbellatus (Pers.) Fr. and ethanol extracts of Alisma plantago-aquatica L. have significant diuretic effects.[22,23] Draba nemorosa L. has a cardiotonic effect.[24] Therefore, it can be concluded that YXT has a therapeutic effect on HF.

Online pharmacology has combined pharmacology with traditional medicine to promote the transformation of the TCM paradigm. Compared to the overall concept of TCM, network pharmacology stands out for its emphasis on systematization and comprehensive analysis, providing a promising new method for studying complex TCM systems. The discovery of 943 targets of YXT's TCM action in network pharmacy mining intersected 141 DEGs from GEO mining HF. Enrichment analysis of its targets revealed that YXT might improve heart failure symptoms by regulating the combined effects of multiple pathways. By combining network pharmacology and high-performance liquid chromatography fingerprint analysis to identify the components of YXT, it can be concluded that the main components were hydroxysafflor yellow A, calycosin-7-O-β-D-glucoside, salvianolic acid B, calycosin, and formaronetin. Xuebijing injection can suppress the NF-κB signaling pathway, reducing IL-6, TNF-α, and IL-1β levels. The expression of inflammatory factors can improve the cardiac function of mice with detoxification syndrome, protect myocardial cells,

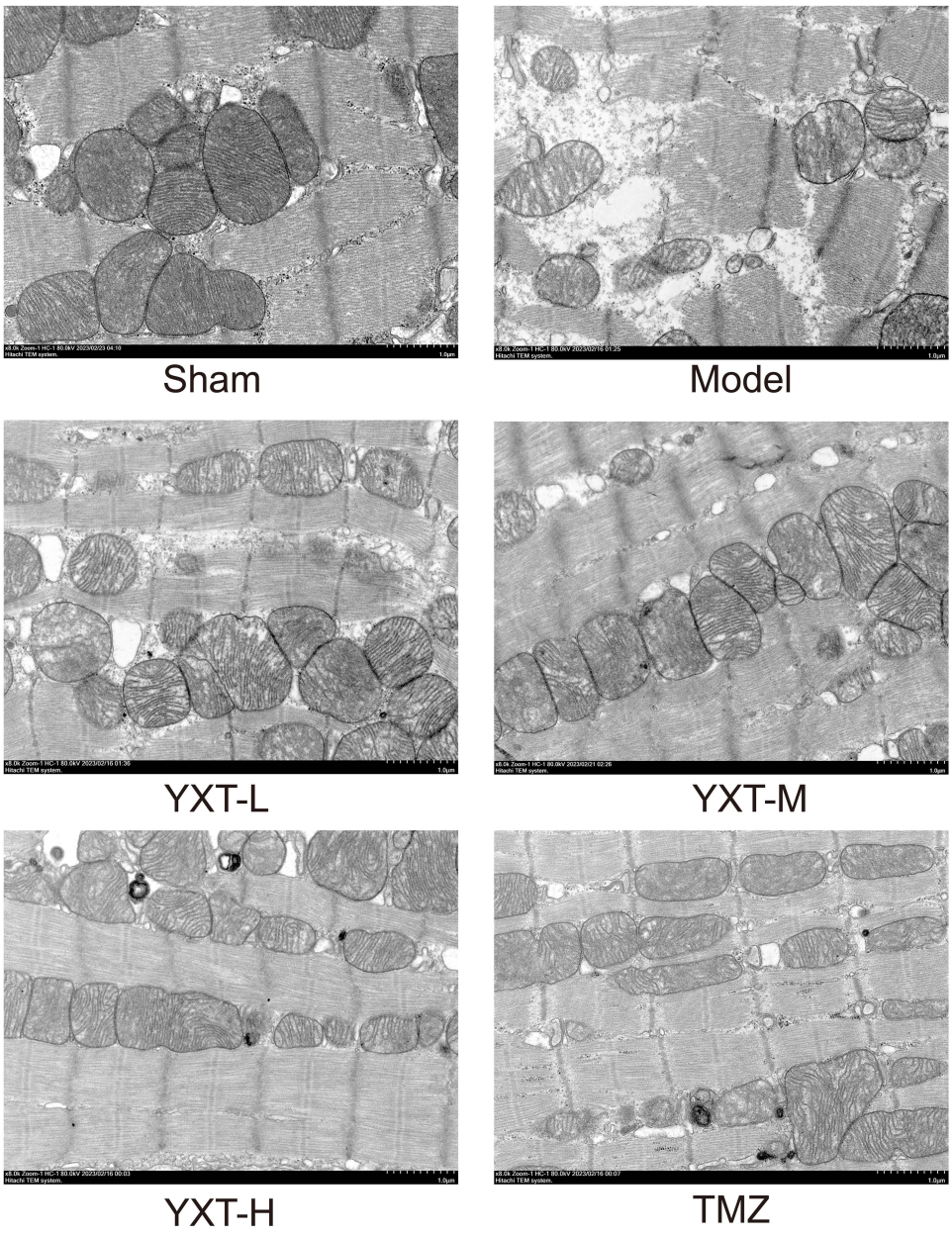

Figure 10 Morphological structure diagram of mitochondria in rat cardiomyocytes (× 3000).

and increase the survival rate. Hydroxysafflor yellow A is the main active compound in Xuebijing injections.[25] Calycosin-7-O-β-D-glucoside (CG) can activate the JAK2/STAT3 signaling pathway by upregulating IL-10 secretion, thereby reducing myocardial cell apoptosis.[26] Salvianolic acid B can alleviate angiotensin II–induced myocardial fibrosis by inhibiting the NF-κB pathway.[27] Calycosin can alleviate myocardial fibrosis and cardiac dysfunction in mice after myocardial infarction by inhibiting the TGFBR1 signaling pathway.[28] Formaronetin can significantly improve cardiac dysfunction, reduce infarct size, and release cardiac markers and TNF in a rat model of myocardial ischemia/reperfusion (I/R)-α, IL-1β, and IL-6 elevation.[29] GO analysis and KEGG enrichment showed that YXT mainly participates in signaling pathways, such as apoptotic calcium signaling, NF-κB signaling, and Toll-like receptors, to intervene in HF. YXT can mediate the PKC/NF-κB signaling pathway and downregulate core DEG expression, thereby alleviating HF. The differentially expressed genes involved in HF intervention through the PRKCB/NF-κB signaling pathway mediated by YXT included ZAP70, TNF, ICAM1, PRKCB, BIRC2, IL1B, and VCAM1.

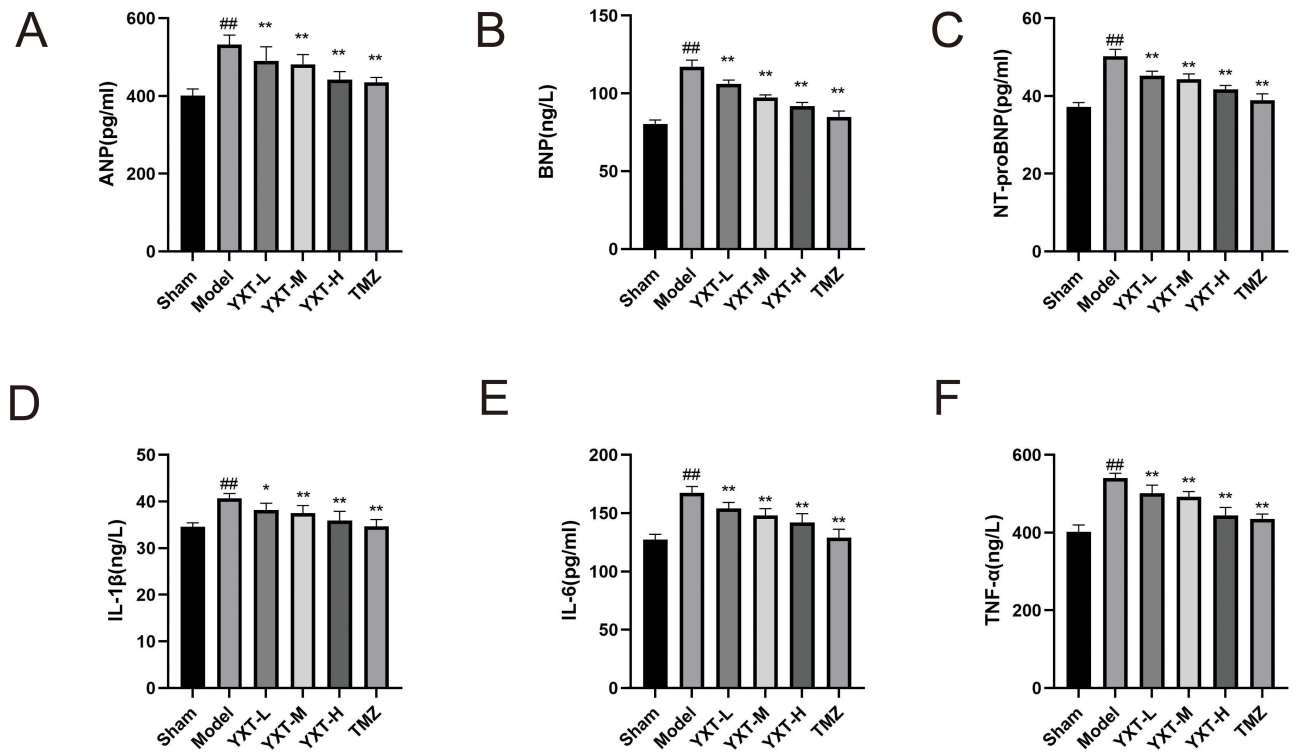

Figure 11 YXT's effect on ANP, BNP, NT-pro BNP, IL-1β, IL-6, and TNF-α levels in HF rats of each group. (**A**) serum ANP content. (**B**) serum BNP content. (**C**) serum NT-pro BNP content. (**D**) serum IL-1β content. (**E**) serum IL-6 content. (**F**) serum TNF-α content.n=6 $^{\#\#}P<0.01$ vs Sham group. $^{**}P<0.01$ vs model group; $^{*}P<0.05$ vs model group. All values are indicated as mean ± SD.

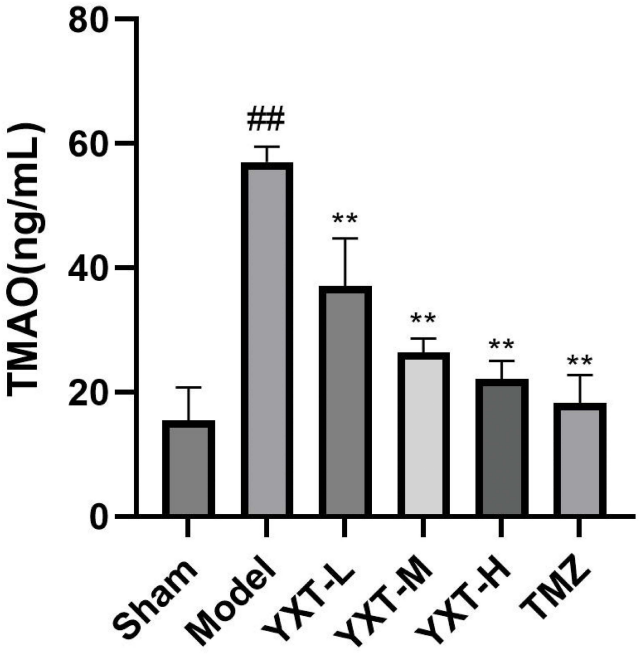

Figure 12 Effect of YXT on TMAO levels in HF rats. $^{\#\#}P<0.01$ vs sham group; $^{**}P<0.01$ vs model group. model group. All values are indicated as mean ± SD.

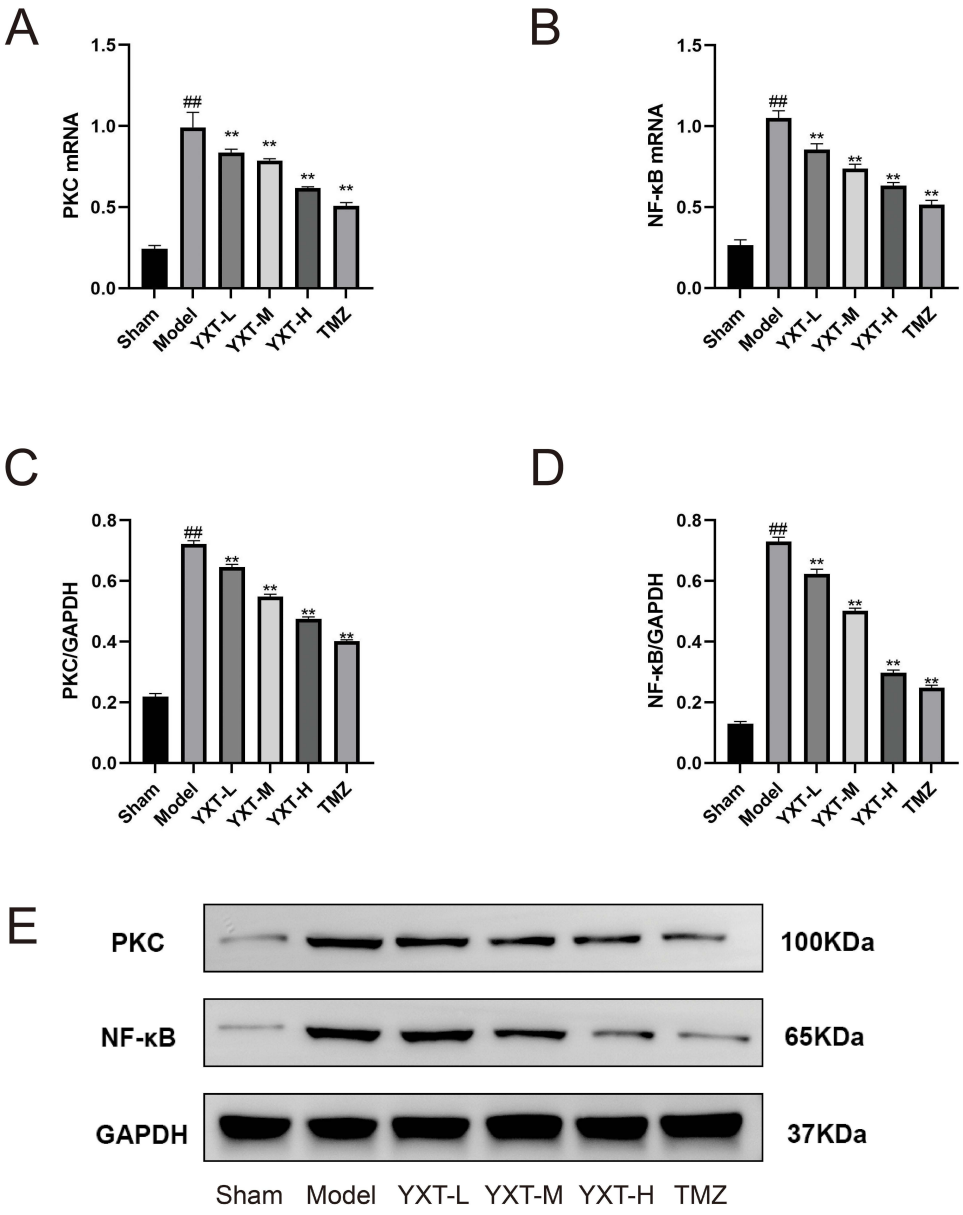

Figure 13 Effects of YXT on NF-κB/PKC signaling pathway in HF rates; (**A**) PKC mRNA expression. (**B**) NF-κB p65 mRNA expression. (**C**) Relative protein expression of PKC. (**D**) Relative protein expression of NF-κB. (**E**) Protein analysis of six groups detected the protein expression of PKC and NF-κB. n=5. $^{\#\#}P<0.01$ vs sham group; $^{**}P<0.01$ vs model group. All values are indicated as mean ± SD.

As an upstream kinase of NF-κB, PKC can activate NF-κB and regulate downstream target gene expression by promoting its phosphorylation and dissociation.[30] PKCs contribute to collagen buildup and fibrosis,[31] whereas NF-κB signaling pathway activation contributes to the pathophysiology of inflammation.[32] Studies in animal models of ischemia and HF have also shown that NF-κB activation and TNF-α are closely related to cardiac hypertrophy, and PKC overexpression can induce the expression of proto-oncogenes, such as c-Fos and c-Jun, leading to increased expression of activator protein 1 (AP-1). The transcription of type IV collagen, fibronectin, and transforming growth factor-β by AP-1 may reduce cardiomyocyte contractility and permeability. This causes extracellular stromal changes, leading to cardiomyocyte hypertrophy, cardiac microangiopathy, and fibrosis of the interstitial material, eventually leading to HF.[33] Inflammation promotes and aggravates HF.[34] Elevated IL-1 and IL-6 levels also increase the risk of heart failure.[35,36] TMAO promotes the activation of PKC/NF-κB,[5,11] releasing cytokines TNF-α, IL-1, and IL-6, inducing an inflammatory

response, leading to myocardial hypertrophy, fibrosis, and HF. Therefore, blocking these signaling pathways may provide new ways to treat HF.

This study found that YXT could improve cardiac function, and the inhibitory effect of YXT on myocardial hypertrophy and fibrosis was observed using HE and Masson's staining. Electron microscopy indicated that YXT could improve myocardial ultrastructure, and serum levels of IL-1β, IL-6, TNF-α, and other inflammatory factors were simultaneously decreased. Together, YXT significantly inhibited NF-κB and PKC expression, suggesting that regulating TMAO/PKC/NF-κB signaling pathway is crucial for the protective effect of YXT in HF. Our results showed that YXT significantly improved cardiac function, reduced myocardial fibrosis, and reduced the levels of intestinal microbiota metabolites and inflammatory factor indicators. Its protective effect was mediated by the activation of the TMAO/PKC/NF-κB signaling pathway. YXT considerably reduced the concentration of TMAO, an intestinal flora metabolite, in the serum of myocardial infarction rats, showing that it can limit pathological changes in HF by lowering TMAO and other intestinal flora metabolites.

Trimetazidine was used as the positive control in this study. Our findings suggest that trimetazidine significantly improves heart function and is capable of inducing cardiac fibrosis, which is consistent with other studies. Trimetazidine can improve intestinal flora metabolites and inflammatory factors and affect the TMAO/PKC/NF-κB signaling pathway. Zhou et al found that trimetazidine significantly reduced the levels of serum inflammatory markers (IL-1β, IL-6, and TNF-α).[37] Zhao et al found that trimetazidine improved myocardial fibrosis and diastolic function.[38] Compared to YXT, trimetazidine is more effective in improving the levels of metabolites of intestinal flora, inflammatory factors, and myocardial fibrosis. This may be because YXT has complex components and targets, which can improve the function of various signaling pathways.

Conclusion

This study confirmed the therapeutic effect of YXT on myocardial infarction rats. Combined with network pharmacology, it was concluded that YXT regulates the TMAO/PKC/NF-κB signaling pathway in chronic ischemic heart failure. This study provides a theoretical basis for the clinical application of YXT in treating heart failure.

Abbreviations

YXT, Yixintai; HF, Heart failure; TCM, traditional Chinese medicine; TMAO, Trimetlylamine oxide; PKC, protein kinase C; NF-κB, Nuclear factor kappa-B; PPI, protein-protein interaction; DEGs, differentially expressed genes; KEGG, Kyoto Encyclopedia of Genes and Genomes; HE, hematoxylin and eosin; ELISA, enzyme-linked immunosorbent assay; PCR, Polymerase chain reaction; ANP, atrial natriuretic peptide; BNP, Brain Natriuretic Peptide; TNF-α, tumour necrosis factor alpha; IL-6, interleukin-6; IL-1β, interleukin-1β; EF, ejection fraction; FS, fractional shortening; VCAM-1, vascular cell adhesion molecule-1; ICAM-1, intercellular cell adhesion molecule-1; BIRC2, baculoviral IAP repeat-containing 2; ZAP70, zeta-associated protein 70; UPLC-MS/MS, ultra-performance liquid chromatography-tandem mass spectrometry; TEM, transmission electron microscope; HPLC, high-performance liquid chromatography; PB, phosphate buffer.

Ethics Statement

All animal experiments were ethically approved by the Animal Experiment Ethics Review Committee of Hunan University of Chinese Medicine (Number: LL2022030207). All the animal care and experimental procedures follow the Guidelines for the Care and Use of Laboratory Animals developed by the Ministry of Science and Technology of China, and the Animal Experiment Ethics Committee of the Hunan University of Chinese Medicine, and all methods are reported in accordance with ARRIVE guidelines for the reporting of animal experiments.

The study involved human data from two public databases, Genecards and GEO. Due to the fact that GeneCards and GEO belong to public databases and users can download relevant data for free for research and publish relevant articles, the Medical Ethics Committee of The First Hospital of Hunan University of Chinese Medicine confirms that this study would have had the need for ethics approval waived.

Acknowledgments

We are very grateful to the staff of Hunan University of Chinese Medicine for their help in the research process. In addition, we are very grateful to the members of the research team for their efforts in the experiment.

Author Contributions

All authors made a significant contribution to the work reported, whether that is in the conception, study design, execution, acquisition of data, analysis and interpretation, or in all these areas; took part in drafting, revising or critically reviewing the article; gave final approval of the version to be published; have agreed on the journal to which the article has been submitted; and agree to be accountable for all aspects of the work.

Funding

This work was supported by the National Natural Science Foundation of China (No.82174343 and No. 81673955), Key R&D Plan of Hunan Province (No. 2022SK2012) and Innovation Project for Graduate Students at Hunan University of Traditional Chinese Medicine (No.2022CX30).

Disclosure

The authors declare no competing interests in this work.

References

1. Tian J, Yan J, Zhang Q, et al. Analysis Of Re-Hospitalizations For Patients With Heart Failure Caused By Coronary Heart Disease: data Of First Event And Recurrent Event. *Ther Clin Risk Manag*. 2019;15:1333–1341. doi:10.2147/TCRM.S218694
2. Rossignol P, Hernandez AF, Solomon SD, Zannad F. Heart failure drug treatment. *Lancet*. 2019;393(10175):1034–1044. doi:10.1016/S0140-6736(18)31808-7
3. Benjamin EJ, Blaha MJ, Chiuve SE, et al. Heart Disease and Stroke Statistics-2017 Update: a Report From the American Heart Association. *Circulation*. 2017;135(10):e146–e603. doi:10.1161/CIR.0000000000000485
4. Seferović PM, Vardas P, Jankowska EA, et al. The Heart Failure Association Atlas: heart Failure Epidemiology and Management Statistics 2019. *Eur J Heart Fail*. 2021;23(6):906–914. doi:10.1002/ejhf.2143
5. Tang W, Li DY, Hazen SL. Dietary metabolism, the gut microbiome, and heart failure. *Nat Rev Cardiol*. 2019;16(3):137–154. doi:10.1038/s41569-018-0108-7
6. Zhang Y, Wang Y, Ke B, Du J. TMAO: how gut microbiota contributes to heart failure. *Transl Res*. 2021;228:109–125. doi:10.1016/j.trsl.2020.08.007
7. Shi R, Re D, Dudl E, et al. Chemical biology strategy reveals pathway-selective inhibitor of NF-kappaB activation induced by protein kinase C. *ACS Chem Biol*. 2010;5(3):287–299. doi:10.1021/cb9003089
8. Seldin MM, Meng Y, Qi H, et al. Trimethylamine N-Oxide Promotes Vascular Inflammation Through Signaling of Mitogen-Activated Protein Kinase and Nuclear Factor-κB. *J Am Heart Assoc*. 2016;5(2). doi:10.1161/JAHA.115.002767
9. Xu GR, Zhang C, Yang HX, et al. Modified citrus pectin ameliorates myocardial fibrosis and inflammation via suppressing galectin-3 and TLR4/MyD88/NF-κB signaling pathway. *Biomed Pharmacother*. 2020;126:110071. doi:10.1016/j.biopha.2020.110071
10. Lee CY, Park HK, Lee BS, et al. Novel Therapeutic Effects of Pterosin B on Ang II-Induced Cardiomyocyte Hypertrophy. *Molecules*. 2020;25(22):5279. doi:10.3390/molecules25225279
11. Ma G, Pan B, Chen Y, et al. Trimethylamine N-oxide in atherogenesis: impairing endothelial self-repair capacity and enhancing monocyte adhesion. *Biosci Rep*. 2017;37(2). doi:10.1042/BSR20160244
12. Jiashuo WU, Fangqing Z, Zhuangzhuang LI, Weiyi J, Yue S. Integration strategy of network pharmacology in Traditional Chinese Medicine: a narrative review. *J Tradit Chin Med*. 2022;42(3):479–486. doi:10.19852/j.cnki.jtcm.20220408.003
13. Ya L, Zou SL, Yi LJ, et al. Research of HPLC fingerprint of Yixintai granule [J]. *Chin J Pharm Anal*. 2021;41(07):1155–1162.
14. Riehle C, Bauersachs J. Small animal models of heart failure. *Cardiovasc Res*. 2019;115(13):1838–1849. doi:10.1093/cvr/cvz161
15. Tang W, Bäckhed F, Landmesser U, Hazen SL. Intestinal Microbiota in Cardiovascular Health and Disease: JACC State-of-The-Art Review. *J Am Coll Cardiol*. 2019;73(16):2089–2105. doi:10.1016/j.jacc.2019.03.024
16. Yazaki Y, Salzano A, Nelson CP, et al. Geographical location affects the levels and association of trimethylamine N-oxide with heart failure mortality in BIOSTAT-CHF: a post-hoc analysis. *Eur J Heart Fail*. 2019;21(10):1291–1294. doi:10.1002/ejhf.1550
17. Wan S, Cui Z, Wu L, et al. Ginsenoside Rd promotes omentin secretion in adipose through TBK1-AMPK to improve mitochondrial biogenesis via WNT5A/Ca(2+) pathways in heart failure. *Redox Biol*. 2023;60:102610. doi:10.1016/j.redox.2023.102610
18. Liu Y, Xu W, Xiong Y, Du G, Qin X. Evaluations of the effect of HuangQi against heart failure based on comprehensive echocardiography index and metabonomics. *Phytomedicine*. 2018;50:205–212. doi:10.1016/j.phymed.2018.04.027
19. Wang L, Yu J, Fordjour PA, et al. Danshen injection prevents heart failure by attenuating post-infarct remodeling. *J Ethnopharmacol*. 2017;205:22–32. doi:10.1016/j.jep.2017.04.027
20. Han CK, Tien YC, Jine-Yuan Hsieh D, et al. Attenuation of the LPS-induced, ERK-mediated upregulation of fibrosis-related factors FGF-2, uPA, MMP-2, and MMP-9 by Carthamus tinctorius L in cardiomyoblasts. *Environ Toxicol: Int J*. 2017;32(3):754–763. doi:10.1002/tox.22275
21. Wu ZL, Ren H, Lai WY, et al. Sclederma of Poria cocos exerts its diuretic effect via suppression of renal aquaporin-2 expression in rats with chronic heart failure. *J Ethnopharmacol*. 2014;155(1):563–571. doi:10.1016/j.jep.2014.05.054
22. Zhang G, Zeng X, Han L, Wei JA, Huang H. Diuretic activity and kidney medulla AQP1, AQP2, AQP3, V2R expression of the aqueous extract of sclerotia of Polyporus umbellatus FRIES in normal rats. *J Ethnopharmacol*. 2010;128(2):433–437. doi:10.1016/j.jep.2010.01.032
23. Chen DQ, Feng YL, Tian T, et al. Diuretic and anti-diuretic activities of fractions of Alismatis rhizoma. *J Ethnopharmacol*. 2014;157:114–118. doi:10.1016/j.jep.2014.09.022

24. Kim SJ, Kim HY, Lee YJ, et al. Ethanol Extract of Lepidium apetalum Seed Elicits Contractile Response and Attenuates Atrial Natriuretic Peptide Secretion in Beating Rabbit Atria. *Evid Based Complement Alternat Med*. 2013;2013:404713. doi:10.1155/2013/404713
25. Wang XT, Peng Z, An YY, et al. Paeoniflorin and Hydroxysafflor Yellow A in Xuebijing Injection Attenuate Sepsis-Induced Cardiac Dysfunction and Inhibit Proinflammatory Cytokine Production. *Front Pharmacol*. 2020;11:614024. doi:10.3389/fphar.2020.614024
26. Liu Y, Che G, Di Z, Sun W, Tian J, Ren M. Calycosin-7-O-β-D-glucoside attenuates myocardial ischemia-reperfusion injury by activating JAK2/STAT3 signaling pathway via the regulation of IL-10 secretion in mice. *Mol Cell Biochem*. 2020;463(1–2):175–187. doi:10.1007/s11010-019-03639-z
27. Wang C, Luo H, Xu Y, Tao L, Chang C, Shen X. Salvianolic Acid B-Alleviated Angiotensin II Induces Cardiac Fibrosis by Suppressing NF-κB Pathway In Vitro. *Med Sci Monit*. 2018;24:7654–7664. doi:10.12659/MSM.908936
28. Chen G, Xu H, Xu T, et al. Calycosin reduces myocardial fibrosis and improves cardiac function in post-myocardial infarction mice by suppressing TGFBR1 signaling pathways. *Phytomedicine*. 2022;104:154277. doi:10.1016/j.phymed.2022.154277
29. Wang DS, Yan LY, Yang DZ, et al. Formononetin ameliorates myocardial ischemia/reperfusion injury in rats by suppressing the ROS-TXNIP-NLRP3 pathway. *Biochem Biophys Res Commun*. 2020;525(3):759–766. doi:10.1016/j.bbrc.2020.02.147
30. Zheng J, Kong C, Yang X, Cui X, Lin X, Zhang Z. Protein kinase C-α (PKCα) modulates cell apoptosis by stimulating nuclear translocation of NF-kappa-B p65 in urothelial cell carcinoma of the bladder. *BMC Cancer*. 2017;17(1):432. doi:10.1186/s12885-017-3401-7
31. Bhattacharjee N, Khanra R, Dua TK, et al. Family: asparagaceae) Attenuates Type 2 Diabetes and Its Associated Cardiomyopathy. *PLoS One*. 2016;11(11):e0167131. doi:10.1371/journal.pone.0167131
32. Khanra R, Dewanjee S, Dua TK, Bhattacharjee N. Taraxerol, a pentacyclic triterpene from Abroma augusta leaf, attenuates acute inflammation via inhibition of NF-κB signaling. *Biomed Pharmacother*. 2017;88:918–923. doi:10.1016/j.biopha.2017.01.132
33. Wang M, Zhang WB, Zhu JH, Fu GS, Zhou BQ. Breviscapine ameliorates hypertrophy of cardiomyocytes induced by high glucose in diabetic rats via the PKC signaling pathway. *Acta Pharmacol Sin*. 2009;30(8):1081–1091. doi:10.1038/aps.2009.95
34. Zuurbier CJ, Abbate A, Cabrera-Fuentes HA, et al. Innate immunity as a target for acute cardioprotection. *Cardiovasc Res*. 2019;115(7):1131–1142. doi:10.1093/cvr/cvy304
35. Abbate A, Toldo S, Marchetti C, Kron J, Van Tassell BW, Dinarello CA. Interleukin-1 and the Inflammasome as Therapeutic Targets in Cardiovascular Disease. *Circ Res*. 2020;126(9):1260–1280. doi:10.1161/CIRCRESAHA.120.315937
36. Ridker PM, Rane M. Interleukin-6 Signaling and Anti-Interleukin-6 Therapeutics in Cardiovascular Disease. *Circ Res*. 2021;128(11):1728–1746. doi:10.1161/CIRCRESAHA.121.319077
37. Zhou X, Li C, Xu W, Chen J. Trimetazidine protects against smoking-induced left ventricular remodeling via attenuating oxidative stress, apoptosis, and inflammation. *PLoS One*. 2012;7(7):e40424. doi:10.1371/journal.pone.0040424
38. Zhao Y, Li S, Quan E, et al. Trimetazidine inhibits cardiac fibrosis by reducing reactive oxygen species and downregulating connective tissue growth factor in streptozotocin-induced diabetic rats. *Exp Ther Med*. 2019;18(2):1477–1485.